Geological Society of America
3300 Penrose Place
P.O. Box 9140
Boulder, CO 80301
(303) 447-2020 • fax 303-357-1073
www.geosociety.org

Geological Society of America
Special Paper 374
2003

Geology and geochronology of granitic batholithic complex, Sinaloa, México: Implications for Cordilleran magmatism and tectonics

Christopher D. Henry
Nevada Bureau of Mines and Geology, University of Nevada, Reno, Nevada 89557, USA

Fred W. McDowell
Department of Geological Sciences, The University of Texas at Austin, Austin, Texas 78712, USA

Leon T. Silver
Division of Geological and Planetary Sciences, California Institute of Technology, Pasadena, California 91125, USA

ABSTRACT

Most of southern Sinaloa is underlain by a large, composite batholith, a continuation of the better-known Cordilleran batholiths of California and Baja California. Field relations and extensive K-Ar and U-Pb dating within a 120-km-wide and 120-km-deep transect show that the Sinaloa batholith formed in several stages. Early layered gabbros have hornblende K-Ar ages of 139 and 134 Ma, although whether these record emplacement age, cooling from metamorphism, or excess Ar is unresolved. A group of relatively mafic tonalites and granodiorites were emplaced before or during an episode of deformation and are restricted to within 50 km of the coast. These plutons, referred to here as syntectonic, show dynamic recrystallization textures that suggest deformation between 300° and 450 °C. A U-Pb zircon date on a probable syntectonic intrusion is 101 Ma. Hornblende K-Ar ages on definite syntectonic intrusions range between 98 and 90 Ma; these may record cooling soon after emplacement or following regional metamorphism.

Numerous posttectonic intrusions crop out from within ~20 km of the coast, where they intrude syntectonic rocks, to the eastern edge of the Sierra Madre Occidental, where they are covered by middle Cenozoic ash-flow tuffs. Posttectonic rocks are dominantly more leucocratic granodiorites and granites. Three samples were analyzed by both U-Pb and K-Ar methods. Their biotite and hornblende ages are concordant at 64, 46, and 19 Ma and agree within analytical uncertainties with U-Pb zircon ages of 66.8, 47.8, and 20 Ma. These data and field relations demonstrate that posttectonic intrusions were emplaced at shallow depths and cooled rapidly. Therefore, concordant K-Ar age pairs and hornblende ages in discordant samples approximate the time of emplacement. Discordance of biotite-hornblende age pairs is largely if not entirely a result of reheating by younger plutons. The combined age data indicate that posttectonic intrusions were emplaced nearly continuously between 90 and 45 Ma. One intrusion is 20 Ma. Based on outcrop area, volumes of intrusions were relatively constant through time.

The combined geochronological data indicate that posttectonic magmatism shifted eastward between 1 and 1.5 km/Ma. Whether syntectonic magmatism also

*E-mails: chenry@unr.edu; mcdowell@mail.utexas.edu; lsilver@gps.caltech.edu.

Henry, C.D., McDowell, F.W., and Silver, L.T., 2003, Geology and geochronology of granitic batholithic complex, Sinaloa, México: Implications for Cordilleran magmatism and tectonics, *in* Johnson, S.E., Paterson, S.R., Fletcher, J.M., Girty, G.H., Kimbrough, D.L., and Martín-Barajas, A., eds., Tectonic evolution of northwestern México and the southwestern USA: Boulder, Colorado, Geological Society of America Special Paper 374, p. 237–273.

migrated is uncertain. Ages of middle and late Tertiary volcanic rocks indicate that magmatism shifted rapidly (10–15 km/Ma) westward from the Sierra Madre Occidental after ca. 30 Ma.

The Sinaloa batholith is borderline calc-alkalic to calcic. SiO_2 contents of analyzed rocks range from 47 to 74%; the lower limit excluding two gabbros is 54%. Syntectonic rocks are more mafic on average than posttectonic rocks. SiO_2 contents of seven out of nine analyzed syntectonic rocks range narrowly between 59 and 62%, with one each at 65 and 67%. The posttectonic rocks show a wider range from 54 to 74% SiO_2, but only border phases and small intrusions have SiO_2 less than ~63%. Combined with their distribution, these data indicate that intrusions become more silicic eastward. The fact that the 20 Ma intrusion is relatively mafic (61% SiO_2) and lies near the coast with syntectonic rocks indicates that composition is related to location rather than to age.

The Sinaloa batholith shows both marked similarities and differences from batholiths of the Peninsular Ranges, Sonora, Cabo San Lucas (Baja California Sur), and Jalisco. The greatest similarities are in types of intrusions, a common sequence from early gabbro through syntectonic to posttectonic rocks, and general eastward migration of magmatism. However, the end of deformation recorded by syntectonic rocks may be different in each area. Sinaloa rocks show a similar wide range of compositions as rocks of the Peninsular Ranges and Sonora but are more potassic than the calcic Peninsular Ranges. Rare earth element patterns are most like those of the eastern part of the Peninsular Ranges and central part of Sonora, both areas that are underlain by Proterozoic crust or crust with a substantial Proterozoic detrital component. However, southern Sinaloa lies within the Guerrero terrane, which is interpreted to be underlain by accreted Mesozoic crust. The greatest differences are in distance and rate of eastward migration. Published data show that magmatism migrated eastward at ~10 km/Ma across the Peninsular Ranges and Sonora and from Jalisco southeast along the southwestern México coast. The area of slower eastward migration roughly correlates with the location of the Guerrero terrane and of possibly accreted oceanic crust that is no older than Jurassic.

Keywords: batholith, geochronology, tectonics, Cordillera, México, Sinaloa.

INTRODUCTION

The chain of granitic batholiths along the North American Cordillera (Fig. 1) may be its most prominent feature and the most permanent record of plate convergence and related magmatism. Batholiths of the Sierra Nevada and Peninsular Ranges of California and northern Baja California have been extensively studied (e.g., Evernden and Kistler, 1970; Gastil, 1975; Gastil et al., 1975; Krummenacher et al., 1975; Silver et al., 1979; Walawender and Smith, 1980; Baird and Miesch, 1984; Silver and Chappell, 1988; Todd et al., 1988; Walawender et al., 1990, 1991; Bateman, 1992; Ortega-Rivera et al., 1997; Johnson et al., 1999a, 1999b; Tate et al., 1999; Kimbrough et al., 2001; Ortega-Rivera, this volume, Chapter 11), but little has been done on the batholiths of mainland México (Anderson and Silver, 1974; Damon et al., 1983a, b; McDowell et al., 2001). Indeed, as with many aspects of Mexican geology that are critical to a full understanding of the geology and evolution of North America, there seems to be little recognition even of their existence.

The Sinaloa batholith is the southward continuation of the Peninsular Ranges batholith and related granitic rocks in Sonora (Fig. 1). Batholithic rocks of the Cabo San Lucas block at the southern end of the Baja California peninsula and the Jalisco area of southwestern México are a further southward continuation (Gastil et al., 1978; Frizzell, 1984; Frizzell et al., 1984; Aranda-Gómez and Perez-Venzor, 1989; Moran-Zenteno et al., 2000; Schaaf et al., 2000; Kimbrough et al., 2002).

Our geologic map of a 10,000 km^2 area in southern Sinaloa forms the basis for an understanding of granitic magmatism in this part of the Cordillera (Fig. 2; Plate 1 [on the CD-ROM accompanying this volume]; Henry and Fredrikson, 1987). Although semitropical weathering is a problem in Sinaloa, cover by younger rocks is much less than in Sonora. The map area is underlain dominantly by batholithic rocks and extends from the Pacific coast to the Sierra Madre Occidental, where the granitic rocks are covered by largely Oligocene and Miocene ash-flow tuffs. This area constitutes a 120-km-wide and 120-km-deep transect across the batholith and is the only area with a relatively comprehensive map between southern Sonora and Nayarit (Gastil and Krummenacher, 1977; Gastil et al., 1978; Gans, 1997). To supplement data from this area, we also sampled granitic rocks in a reconnaissance transect in northern Sinaloa (Fig. 1). Based

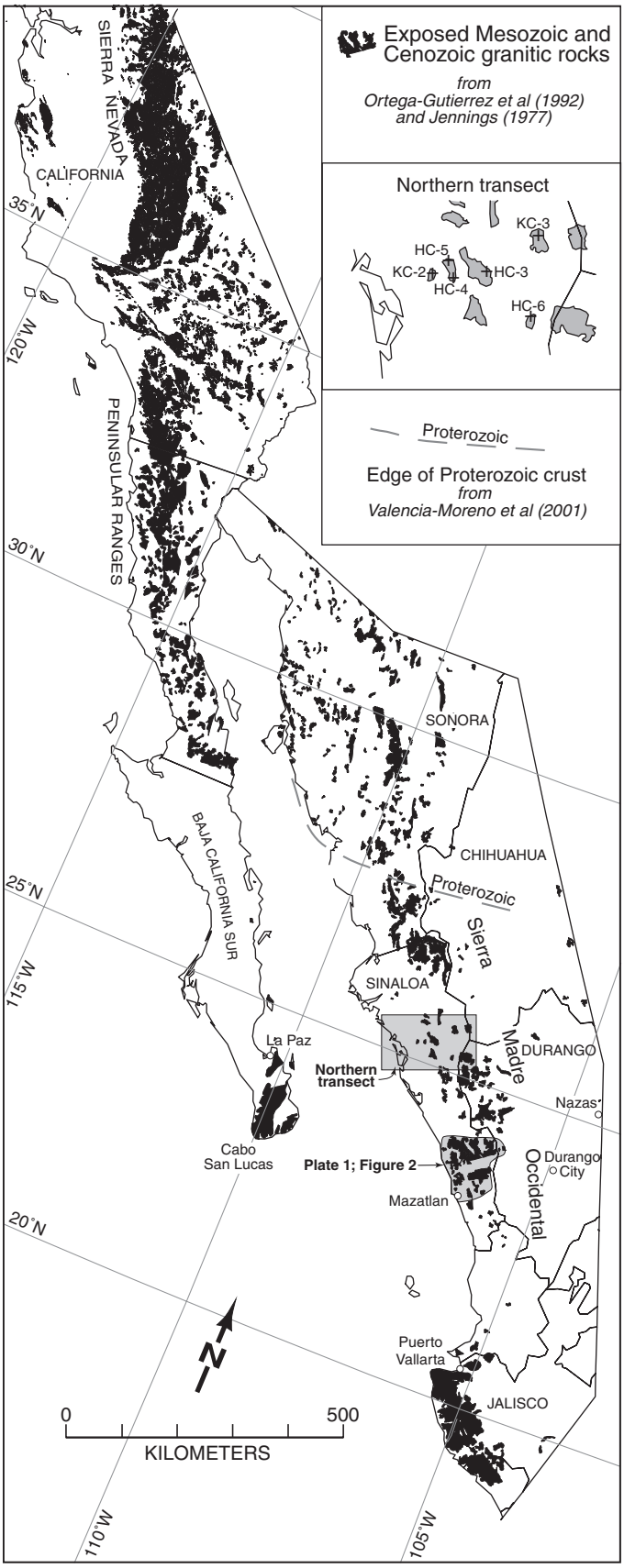

Figure 1. Mesozoic and Cenozoic granitic rocks of southern California and western México (from Jennings, 1977, and Ortega-Gutiérrez et al., 1992). Cretaceous to Tertiary granitic rocks crop out discontinuously from Sierra Nevada through Peninsular Ranges of California and Baja California, to Cabo San Lucas block of Baja California Sur, and through Sonora and Sinaloa to Jalisco. Granitic rocks continue southeast along southern México coast (Schaaf et al., 1995; Moran-Zenteno et al., 2000). They once formed a continuous belt that has been disrupted by displacement along San Andreas and other major faults and by seafloor spreading in Gulf of California. Shaded areas denote area of Figure 2 and northern Sinaloa transect. Northern transect is blown up to show sample locations.

upon this mapping we have acquired an extensive suite of K-Ar and U-Pb data that are critical to understanding the character and development of the Sinaloa batholith.

Locations mentioned here variably cite them relative to Mazatlan, for reference to the simplified geologic map of Figure 2, or more precisely in reference to Plate 1, the more detailed geologic map of Henry and Fredrikson (1987).

GEOCHRONOLOGY AND COMPARISON OF K-AR AND U-PB DATA

Fifty-seven samples representing a large but unknown number of separate granitic intrusions and seven samples of minor intrusions or volcanic rocks were dated by the K-Ar method; both biotite and hornblende were analyzed in 34 of these (Table 1, Appendix 1). Fifty-one of the granitic samples and all of the minor rocks are from the map area in southern Sinaloa, with a concentration of data from a well-constrained, east-northeast transect along the Rio Piaxtla (Plate 1, Fig. 2). The other six dated samples are from the northern reconnaissance transect (Fig. 1). Four samples that spanned most of the range of K-Ar ages and include both syn- and posttectonic intrusions were further dated by U-Pb on zircon (Table 2, Appendix 1). K-Ar ages range from ca. 145 Ma to 19 Ma, but, as explained below, the oldest apparent age probably reflects excess Ar. U-Pb ages on the four samples, ca. 101, 67, 48, and 20 Ma, are critical for establishing the overall age range and significance of K-Ar ages.

If biotite and hornblende ages from a single sample are indistinguishable within analytical uncertainty, we consider them to be concordant. By this criterion, twenty-one biotite-hornblende pairs in Table 1 are concordant. Samples with younger ages are more commonly concordant than are samples with older ages. Geologic inferences drawn from concordant results depend largely upon the age of the rock in question. A small absolute age difference for a relatively young (e.g., 50 Ma) rock implies rapid cooling from ~500 °C through ~300 °C (the estimated blocking temperatures for hornblende and biotite; Harrison, 1981; Harrison et al., 1985). In most cases, such rapid cooling would immediately follow emplacement. A granitic intrusion emplaced at great depth might stay at elevated temperature for

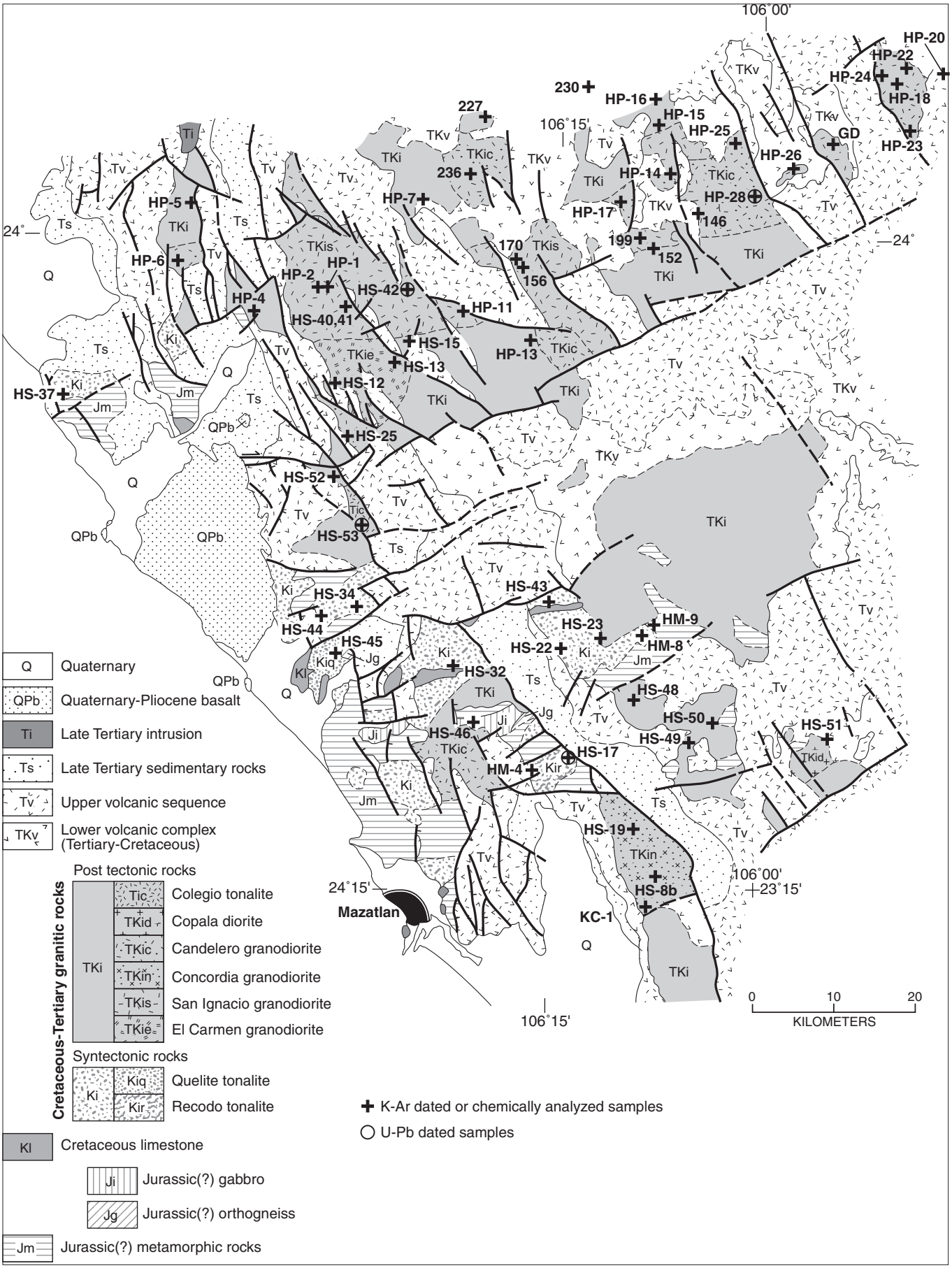

Figure 2. Simplified geologic map of southern Sinaloa showing locations of isotopically dated or chemically analyzed samples (from Henry and Fredrikson, 1987; see Plate 1 for detailed map).

TABLE 1. K-Ar DATA

Sample	Rock type	Mineral[1]	% K	$^{40}Ar^{*}$ ($x10^{-5}$ scc/gm)	% $^{40}ArRad$	Age[2] (Ma)	±1σ
Gabbro (Jm)							
HS-46	Gabbro	H	0.158	0.0801	61.8	**133.8**	3.0
			0.146	0.0832	57.2		
			0.150				
HS-48	Gabbro	H	0.427	0.2392	73.0	**138.6**	3:1
			0.423	0.2365	70.2		
Syntectonic Intrusions (Ki)							
HS-17	Recodo tonalite	B	6.50	1.329	74.4	**52.7**	0.6
			6.44	1.359	90.4		
		H #1	0.350	0.1885	72.3	**125.0**	10.1
			0.362	0.1682	55.1		
			0.352				
		H #2	0.347	0.1904	65.8	**130.5**	2.9
			0.365				
			0.374				
			0.360				
		P	0.195	0.1116	55.6	**145.4**	3.3
			0.185				
			0.189				
HM-4	Recodo tonalite	B	6.75	2.649	92.7	**98.3**	1.1
			6.68	2.621	92.6		
		H	0.720	0.2794	85.1	**96.3**	2.2
			0.733				
			0.729				
HS-43	Amphibolite	H	0.745	0.2837	76.4	**94.5**	1.1
			0.756				
			0.756				
HS-22	Foliated granodiorite	B	7.06	2.564	94.5	**91.3**	1.0
			7.02	2.557	89.0		
		H	0.552	0.2177	89.4	**97.9**	2.2
			0.565				
			0.553				
HM-8	Quartz diorite	B	6.82	1.853	84.5	**69.0**	0.8
			6.74				
		H	0.664	0.2540	86.9	**95.6**	2.1
			0.668				
HS-45	Quelite tonalite	B	7.41	2.369	94.3	**80.7**	0.9
			7.36				
		H	0.855	0.3225	92.1	**94.3**	2.1
			0.859				
HS-44	Granodiorite	B	6.92	2.563	90.4	**92.8**	1.0
			6.94	2.564	80.5		
HS-34	Foliated granodiorite	B	6.97	2.511	95.2	**89.8**	1.0
			7.07				
			7.01				
		H	0.781	0.2538	83.5	**86.5**	1.9
			0.774	0.2818	84.7		
KC-2	Gneissic granodiorite	B	6.65	2.377	87.1	**89.7**	1.0
			6.66				
		H	0.525	0.1926	69.9	**93.4**	2.1
			0.510				
HC-4A	Foliated quartz diorite	B	6.82	2.499	90.5	**92.1**	1.0
			6.80				
		H	0.555	0.1984	80.8	**90.4**	2.0
			0.547				
HS-37	Foliated quartz diorite	B	7.10	2.415	90.9	**85.7**	1.0
			7.06				
		H	1.130	0.4030	88.7	**89.1**	2.0
			1.140				

1—B=biotite; H=hornblende; P=pyroxene; A=adularia (with a lot of quartz).
2—Ages calculated with decay constants of Steiger and Jager (1977); ^{40}K = 0.01167 atom percent, λ_{β} = 4.962 x 10^{-10} yr^{-1}; λ_{ϵ} = 0.581 x 10^{-10} yr^{-1}.

(continued)

TABLE 1. K-Ar DATA *(continued)*

Sample	Rock type	Mineral[1]	% K	$^{40}Ar^*$ (x10^{-5} scc/gm)	% ^{40}ArRad	Age[2] (Ma)	±1σ
Syntectonic Intrusions (Ki) *(continued)*							
HS-32	Hypersthene granodiorite	B	6.80	1.8780	86.8	**69.4**	0.8
			6.69				
		P	0.130	0.0439	13.3	**85.8**	1.9
			0.121	0.0440	6.2		
			0.135				
Posttectonic Intrusions (Tki)							
HC-5	Granodiorite	B	6.56	2.321	88.9	**88.6**	1.0
			6.59				
		H	0.659	0.2352	83.6	**89.5**	2.0
			0.660				
HS-12	El Carmen granodiorite	B	6.61	1.946	88.2	**75.0**	0.8
			6.54	1.964	91.6		
		H	0.696	0.1953	65.5	**73.0**	1.6
			0.687	0.2048	88.9		
HS-13	El Carmen granodiorite	B	6.42	1.604	82.7	**62.9**	0.7
			6.47				
		H	0.650	0.1922	55.6	**74.7**	1.7
			0.648				
HS-25	El Carmen granodiorite	B	1.98	0.5085	77.0	**65.2**	0.7
			1.96				
		H	0.372	0.1090	74.9	**73.4**	1.6
			0.377				
HS-50	Quartz diorite	B	5.60	1.493	8.0	**67.2**	0.8
			5.61		.		
		H	0.502	0.1405	65.4	**70.6**	1.6
			0.502				
HC-6	Monzogranite	B	4.88	1.277	85.0	**65.9**	0.8
			4.92				
		H	0.515	0.1365	65.9	**67.4**	1.5
			0.508				
HS-15	Granodiorite	B	5.62	1.411	83.7	**63.7**	0.7
			5.60	1.415	92.2		
		H	0.506	0.1320	79.1	**65.9**	1.4
			0.507				
152	Quartz diorite	B	3.66	0.7215	77.5	**51.3**	0.6
			3.53				
			3.52				
		H	0.437	0.1157	73.2	**67.1**	1.5
			0.434				
HP-4	Quartz diorite	B	6.77	1.724	81.4	**64.4**	0.7
			6.76	1.722	91.3		
		H	0.447	0.1138	67.7	**64.7**	1.4
			0.452	0.1162	80.9		
HS-42	San Ignacio granodiorite main San Ignacio pluton	B	6.92	1.735	91.6	**63.4**	0.7
			6.93				
		H	0.520	0.1316	52.4	**64.1**	1.4
			0.518				
HS-40	San Ignacio granodiorite main San Ignacio pluton	B	7.32	1.853	91.9	**64.3**	0.7
			7.26				
HS-41	San Ignacio granodiorite main San Ignacio pluton	B	6.94	1.764	93.2	**63.9**	0.7
			7.02				
HP-2	San Ignacio granodiorite main San Ignacio pluton	B	5.71	1.169	81.1	**51.7**	0.6
			5.75				
		H	0.701	0.1757	76.6	**63.7**	1.4
			0.685				
			0.708				

1—B=biotite; H=hornblende; P=pyroxene; A=adularia (with a lot of quartz).
2—Ages calculated with decay constants of Steiger and Jager (1977); ^{40}K = 0.01167 atom percent, $\lambda_\beta = 4.962 \times 10^{-10}$ yr^{-1}; $\lambda_\varepsilon = 0.581 \times 10^{-10}$ yr^{-1}.

(continued)

TABLE 1. K-Ar DATA *(continued)*

Sample	Rock type	Mineral[1]	% K	$^{40}Ar^*$ (x10^{-5} scc/gm)	% ^{40}ArRad	Age[2] (Ma)	±1σ
Posttectonic Intrusions (Tki) ***(continued)***							
HP-11	San Ignacio granodiorite	B	5.78	1.388	83.2	**61.0**	0.7
	main San Ignacio pluton		5.71	1.382	89.5		
		H	0.552	0.1377	64.5	**63.7**	1.4
			0.545	0.1385	77.7		
156	San Ignacio granodiorite	B	6.60	1.672	83.0	**64.6**	0.7
			6.46				
			6.57				
		H	0.610	0.1531	61.4	**63.2**	1.4
			0.615				
170	San Ignacio granodiorite	B	6.20	1.588	86.5	**64.5**	0.7
			6.26				
146	San Ignacio granodiorite	B	6.54	1.207	80.4	**47.0**	0.5
			6.51				
		H	0.564	1.116	63.4	**49.6**	1.1
			0.586				
			0.563				
			0.56				
HP-26	San Ignacio granodiorite	B	6.42	1.245	79.6	**49.3**	0.6
			6.41				
HS-23	Granodiorite	B	5.88	1.446	84.6	**62.1**	0.7
			5.91				
HS-51	Granodiorite	B	4.09	0.9365	80.2	**57.9**	0.7
			4.11				
HM-9	Monzogranite	B	4.68	1.007	83.5	**55.0**	0.6
			4.61				
KC-3	Monzogranite	B	6.86	1.384	84.1	**52.6**	0.6
			6.66				
KC-1	Granodiorite	B	1.74	0.3960	63.3	**57.3**	0.6
			1.76				
HS-8b	Concordia granodiorite	B	4.89	1.045	79.9	**53.8**	0.6
			4.91	1.033	86.2		
		H	0.620	0.1329	56.8	**54.2**	1.2
			0.613	0.1307	82.0		
HP-16	Granodiorite	B	5.80	1.232	85.2	**54.5**	0.6
			5.79	1.261	87.5		
		H	0.515	0.1131	56.4	**55.6**	1.2
			0.516				
230	Granodiorite	B	6.23	1.342	89.4	**53.8**	0.6
			6.29	1.316	91.4		
		H	0.673	0.1443	60.8	**53.6**	1.2
			0.671	0.1398	62.0		
HP-7	Diorite	H	0.238	0.0494	44.4	**52.2**	1.2
			0.242				
HP-5	Granodiorite	B	3.75	0.7798	75.0	**52.4**	0.6
			3.80				
HP-15	Granodiorite	B	7.27	1.363	86.3	**47.7**	0.5
			7.25				
HP-22	Granodiorite	B	6.87	1.226	87.1	**45.5**	0.5
			6.88	1.234	89.6		
		H	0.526	0.0936	52.0	**46.2**	1.0
			0.524	0.0974	54.2		
HP-6	Candelero granodiorite	B	5.77	1.907	89.3	**81.8**	0.9
			5.83	1.864	90.3		
		H	0.634	0.2078	76.6	**82.6**	1.8
			0.633	0.2083	81.3		

1—B=biotite; H=hornblende; P=pyroxene; A=adularia (with a lot of quartz).
2—Ages calculated with decay constants of Steiger and Jager (1977); ^{40}K = 0.01167 atom percent, $\lambda_\beta = 4.962 \times 10^{-10}$ yr^{-1}; $\lambda_\varepsilon = 0.581 \times 10^{-10}$ yr^{-1}.

(continued)

TABLE 1. K-Ar DATA *(continued)*

Sample	Rock type	Mineral[1]	% K	$^{40}Ar^*$ ($x10^{-5}$ scc/gm)	% $^{40}ArRad$	Age[2] (Ma)	±1σ
Posttectonic Intrusions (Tki) *(continued)*							
HP-13	Candelero granodiorite	B	6.45	1.564	73.3	**61.3**	0.7
			6.47				
		H	0.722	0.1770	69.3	**62.0**	1.4
			0.705				
			0.740				
236	Candelero granodiorite	B	2.29	0.5099	66.3	**52.4**	5.1
			2.33	0.4436	75.1		
		H	0.338	0.0698	46.9	**51.2**	1.6
			0.339	0.0668	58.8		
HC-3	Candelero granodiorite	B	4.87	0.9829	80.5	**51.2**	0.6
			4.88				
		H	0.336	0.0654	51.9	**49.7**	1.1
			0.328				
			0.339				
HP-14	Candelero granodiorite main Candelero pluton	B	4.20	0.7605	75.7	**47.0**	0.5
			4.08	0.7727	83.4		
		H	0.480	0.0876	39.2	**46.6**	1.0
			0.475				
HP-25	Candelero granodiorite main Candelero pluton	B	6.26	1.134	76.8	**46.4**	0.5
			6.15				
HP-28	Candelero granodiorite main Candelero pluton	B	6.18	1.115	91.4	**46.0**	0.5
			6.14				
		H	0.352	0.0613	53.2	**44.6**	1.0
			0.348	0.0615	38.5		
HP-18	Candelero granodiorite	B	4.59	0.7919	66.7	**43.9**	0.5
			4.58				
HP-23	Candelero granodiorite	B	6.01	0.7842	70.6	**33.5**	0.4
			5.93				
HP-20	Candelero granodiorite	B	3.92	0.4770	66.7	**30.9**	0.3
			3.96				
199	Quartz diorite	B	6.53	1.267	83.4	**49.3**	0.6
			6.52				
GD	Granodiorite	B	2.24	0.3883	58.4	**43.8**	0.5
			2.27				
Hbl por	Porphyritic granodiorite	H	0.415	0.0771	60.3	**47.5**	1.0
			0.410				
227	Granodiorite	B	4.58	0.5210	59.0	**29.1**	0.3
			4.56				
HS-53	Colegio tonalite	B	7.54	0.5467	65.4	**18.7**	0.2
			7.45				
		H #1	0.609	0.0468	39.8	**19.5**	0.4
			0.651	0.0494	54.3		
			0.629				
			0.639				
		H #2	0.525	0.0401	53.4	**19.0**	0.4
			0.530	0.0381	43.0		
Upper volcanic rocks							
HP-24	quartz diorite dike	B	6.76	0.8473	76.4	**31.8**	0.4
			6.80	0.8400	78.0		
HP-10	andesite dike	H	0.490	0.0565	58.1	**29.5**	0.7
			0.488				
174	rhyolite dike	B	4.65	0.4357	38.7	**23.8**	0.3
			4.71				
HM-1	dacite lava	B	5.20	0.4501	66.8	**22.3**	0.2
			5.13				
Miscellaneous							
Adularia	Vein	A	0.597	0.0947	46.9	**40.9**	0.4
			0.593	0.0965	50.1		

1—B=biotite; H=hornblende; P=pyroxene; A=adularia (with a lot of quartz).
2—Ages calculated with decay constants of Steiger and Jager (1977); ^{40}K = 0.01167 atom percent, $\lambda_\beta = 4.962 \times 10^{-10}$ yr^{-1}; $\lambda_\varepsilon = 0.581 \times 10^{-10}$ yr^{-1}.

TABLE 2. U-Pb DATA

	Zircon weight (mg)	Concentration (ppm)		Observed isotope ratios		Atom ratios[1]			Ages (Ma)[2]		
		U	Pb[1]	$^{206}Pb/^{204}Pb$	$^{207}Pb/^{204}Pb$	$^{206}Pb/^{238}U$	$^{207}Pb/^{235}U$	$^{207}Pb/^{206}Pb$	$^{206}Pb/^{238}U$	$^{207}Pb/^{235}U$	$^{207}Pb/^{206}Pb$
HS-53 Colegio tonalite (best age estimate = 20.0 ± 0.4 Ma)											
Fraction 1											
conc. 1	306.2	206.7	0.899	55.61	17.66	0.00362	0.02889	0.05404	23.3 ± 1.0	26.9 ± 3.0	373 ± 260
conc. 2		203.0	0.777	92.50	19.28	0.00319	0.02172	0.04938	20.5 ± 0.4	21.8 ± 2.5	166 ± 140
Fraction 2											
conc.	594.1	253.7	0.943	96.25	19.29	0.00311	0.02013	0.04705	20.0 ± 0.4	20.2 ± 1.3	52 ± 190
HP-28 Candelero granodiorite (best age estimate = 47.8 ± 1.0 Ma)											
Fraction 1											
conc.	308.6	983.4	7.873	614.09	43.64	0.00748	0.04828	0.04691	48.0 ± 1.0	47.9 ±1.0	46 ± 30
comp.				719.69	48.90			0.04750			
Fraction 2											
conc.	439.1	802.0	6.312	364.88	32.14	0.00740	0.04858	0.04759	47.6 ± 1.0	48.2 ± 1.2	79 ± 40
HS-42 San Ignacio granodiorite (best age estimate = 66.8 ± 1.3 Ma)											
Fraction 1											
conc.	384.4	371.9	4.043	118.68	20.24	0.01035	0.06575	0.04550	66.4 ± 1.3	64.7 ± 3.2	<0 ± >85
Fraction 2											
conc.	187.9	514.7	5.641	149.79	21.86	0.01046	0.06855	0.04770	67.1 ± 1.3	67.3 ± 2.7	84 ± 85
comp.				169.20	22.51			0.04531			
HS-17 Recodo tonalite (best age estimate = 101.2 ± 2.0 Ma)											
Fraction 1											
conc.	270.5	297.2	4.623	191.70	24.19	0.01583	0.10585	0.04901	101.2 ± 2.0	102.2 ± 3.3	148 ± 65
comp.				206.18	24.88			0.04951			
Fraction 2											
conc.	439.1	335.6	5.380	327.70	30.45	0.01581	0.10478	0.04810	101.1 ± 2.0	101.2 ± 2.4	104 ± 40

1—radiogenic; corrected for $^{206}Pb/^{204}Pb$ = 18.60 and $^{207}Pb/^{204}Pb$ = 15.60 for both blank and common Pb.
2—calculated with $^{238}U/^{235}U$ = 137.88; $\lambda 238 = 1.55125 \times 10^{-10}$; $\lambda 235 = 9.8485 \times 10^{-10}$.
conc.—concentration, aliquot spiked with ^{208}Pb and ^{235}U before fusion; comp. = composition, unspiked.

long time, but except in unusual circumstances, it would not then cool rapidly enough to generate concordant ages. For older rocks, e.g., ≥100 Ma, the larger absolute age difference of between 3 and 4 Ma allowed by concordance of our criteria does not allow such a simple explanation. A concordant 100 Ma rock could have cooled relatively slowly following emplacement. Further interpretation must recognize the geologic setting.

The best estimate of the U-Pb age for samples HP-28, HS-42, and HS-17, where both fractions are concordant, is taken to be the average of the two $^{206}Pb/^{238}U$ ages (Table 2). The best estimate of the U-Pb age for sample HS-53, where only fraction 2 is concordant, is taken to be that fractions $^{206}Pb/^{238}U$ age. We choose the $^{206}Pb/^{238}U$ ages because most of the ^{207}Pb in all samples is from the reagents used in analysis, especially the borate flux. Therefore, uncertainties in the $^{207}Pb/^{235}U$ and $^{207}Pb/^{206}Pb$ ages are large. Nevertheless, most $^{206}Pb/^{238}U$ and $^{207}Pb/^{235}U$ ages are indistinguishable within the analytical uncertainties, and only the $^{207}Pb/^{206}Pb$ ages of sample HS-53 differ significantly from the $^{206}Pb/^{238}U$ and $^{207}Pb/^{235}U$ ages. An obvious implication of these data is that the rocks contain little if any inherited zircon.

The U-Pb zircon ages for three posttectonic samples are all slightly greater than but mostly within analytical uncertainties of concordant biotite-hornblende pairs: HS-42 zircon 66.8 ± 1.3 Ma, biotite 63.4 ± 0.7 Ma, hornblende 64.1 ± 1.4 Ma; HP-28 zircon 47.8 ± 1.0 Ma, biotite 46.0 ± 0.5 Ma, hornblende. 44.6 ± 1.0 Ma; HS-53 zircon 20.0 ± 0.04 Ma, biotite 18.7 ± 0.2 Ma, hornblende 19.0 ± 0.4 and 19.5 ± 0.4 Ma (Fig. 3, Tables 1 and 2). Results from the fourth sample, HS-17, which is pre-or syntectonic, are complicated. The U-Pb age is well defined at 101.2 ± 2.0 Ma. The K-Ar biotite age is much younger, at 52.7 ± 0.6 Ma. Apparent ages of three different separates of amphibole-pyroxene mixtures are impossibly old at 125.0 ± 10.1 to 145.4 ± 3.3 Ma. In thin section, hornblende encloses and is intimately intergrown with clinopyroxene and a colorless amphibole, probably tremolite. It was not possible to get pure separates of any phase, but the roughly inverse relation between K and Ar contents (Table 1) suggests that pyroxene contains excess Ar. The high, ~0.19% K content of the pyroxene concentrate indicates significant contamination with another phase, either or both of the amphiboles. The U-Pb and K-Ar results for sample HS-17 can be further illuminated by comparison with K-Ar ages of sample HM-4, which we interpret to be the same intrusion. Sample HM-4, collected just 5.5 km to the west of HS-17, is petrographically and compositionally similar to sample HS-17 (Table 3). The biotite (98.3 ± 1.1 Ma) and hornblende (96.3 ± 2.2 Ma) ages from sample HM-4 are, as with the posttectonic samples, slightly younger than and partly overlap with the U-Pb age.

The general agreement between the K-Ar and U-Pb ages for at least three and possibly all four samples implies that the sampled intrusions cooled rapidly following emplacement. This interpretation is strongest for the posttectonic intrusions, for which 18 of 25 sample pairs are concordant (Fig. 3, Table 1). It is consistent with field observations that infer shallow emplacement for the posttectonic intrusions. They generally intrude and commonly dome possibly contemporaneous volcanic rocks (Lower volcanic complex of Fig. 2 and Plate 1). Contacts are sharp, discordant, and commonly brecciated. The intrusions are locally porphyritic and associated with numerous epithermal ore deposits (Smith et

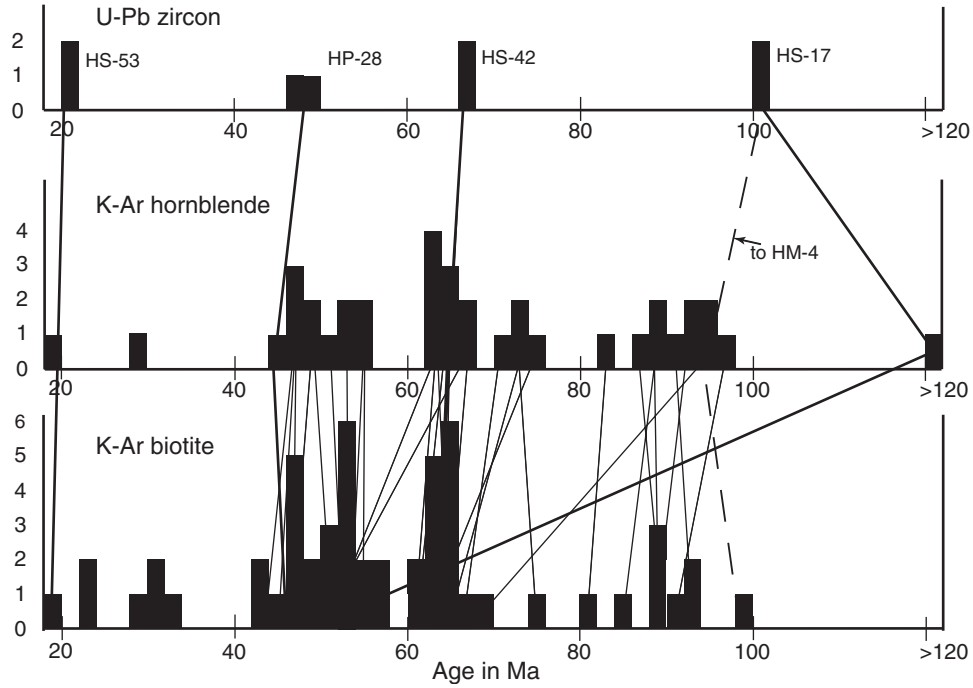

Figure 3. Histogram of U-Pb zircon, K-Ar hornblende, and K-Ar biotite ages. Tie lines connect dates on separates from same samples. Heavy lines connect four samples for which U-Pb dating was employed. Dashed line connects U-Pb age of sample HS-17 to K-Ar ages of sample HM-4, which is from same Recodo tonalite. K-Ar ages are slightly lower but mostly within analytical uncertainties of U-Pb ages. Our interpretation is that concordant biotite and hornblende K-Ar ages, those that agree within analytical uncertainty, generally record rapid cooling immediately following emplacement.

TABLE 3. CHEMICAL ANALYSES OF GRANITIC ROCKS, SINALOA BATHOLITH

	Gabbro		Syntectonic rocks								
Unit:			Quelite tonalite					Recodo tonalite			
Sample:	HS-46	HS-48	HS-37	HS-34	HS-44	HS-45	HS-22	HM-8	HS-17	HM-4	HS-32
Map unit:	Ji	Ji	Ki	Ki	Ki	Kiq	Ki	Ki	Kir	Kir	Ki
SiO_2	47.28	49.34	61.32	64.97	67.19	58.57	60.99	59.25	58.67	60.48	59.86
TiO_2	1.84	2.34	0.87	0.69	0.58	0.79	0.94	0.96	0.91	0.79	0.94
Al_2O_3	23.92	16.08	16.22	15.77	15.48	17.42	16.67	16.85	16.38	15.34	16.41
Fe_2O_3	1.63	12.16	6.65	1.78	2.16	4.77	2.10	0.29	1.90	6.96	1.97
FeO*	6.13			2.71	1.84	2.19	3.97	7.08	5.43		4.17
MnO	0.12	0.20	0.11	0.07	0.04	0.12	0.10	0.12	0.13	0.09	0.10
MgO	2.15	5.98	2.39	2.41	1.94	3.44	2.98	3.64	4.39	3.46	3.81
CaO	12.66	10.19	4.88	4.48	3.69	6.47	5.53	6.03	7.09	5.74	6.03
Na_2O	3.22	1.87	3.56	4.24	4.17	4.07	3.92	3.64	3.25	3.26	4.00
K_2O	0.19	0.71	2.99	2.67	2.76	1.97	2.59	1.90	1.63	2.19	2.46
P_2O_5	0.85	0.08	0.58	0.20	0.15	0.20	0.21	0.25	0.21	0.18	0.24
H_2O+											
H_2O-											
LOI	0.58	1.17	0.41	0.85	1.69	0.93	0.86	0.59	1.69	1.62	0.60
Total*	100.58	100.13	99.97	100.85	101.69	100.93	100.86	100.59	101.69	100.13	100.60
Sc xrf	20	33	17	10	9	20	16	18	25	20	18
V	207	403	119	109	58	175	142	191	177	184	156
Ni	25	<20	44	31	14	27	13	110	28	<20	146
Cu	164	74	19	35	244	60	51	56	35	30	43
Zn	104	98	83	74	36	90	90	96	98	79	80
Ga	24	20	20	20	12	19	19	20	18	19	19
As	5	<5	<5	<5	6	<5	11	8	7	<5	6
Rb	4	21	105	55	57	62	69	56	50	67	48
Sr	705	347	327	647	360	551	520	541	467	405	651
Sr xrf	705	346	336	608	546	529	493	534	439	400	623
Y	25	23.9	28.5	10	5	18	19	19	19	20.4	15
Y xrf	26	23.0	28.0	11	7	20	19	19	18	20.0	16
Zr	65	94	225	157	81	158	284	139	112	155	194
Zr xrf	68	125	236	168	130	139	257	144	115	157	201
Nb	17.6	15.2	7.4	7.3	4.2	7.0	12.5	9.1	7.2	5.3	9.8
Mo	9.0	<2	<2	5.6	13.5	7.3	4.9	9.2	5.7	<2	5.7
Sb	0.9	0.4	-0.2	0.5	0.3	0.3	1.2	3.1	0.8	0.6	0.5
Cs	2.2	3.8	5.0	1.8	3.7	3.1	3.0	2.2	2.4	4.8	1.2
Ba	127	382	991	1070	557	541	863	717	550	712	1083
Ba xrf	134	368	994	1072	882	535	871	731	533	678	1068
La	15.5	16.1	29.4	27.1	12.9	22.2	27.6	21.4	19.6	23.1	26.5
Ce	38.9	35.3	58.3	50.9	23.7	43.3	52.9	45.3	39.3	46.1	51.2
Pr	5.62	4.49	6.96	5.72	2.59	4.97	6.12	5.55	4.59	5.33	5.88
Nd	27.9	18.7	27.5	21.2	9.0	20.1	22.8	22.7	18.4	20.7	22.7
Sm	6.8	4.33	5.84	4.0	1.5	4.2	4.6	4.9	3.9	4.24	4.4
Eu	3.04	1.34	1.22	1.08	0.56	1.19	1.20	1.29	1.20	1.03	1.28
Gd	7.1	4.06	5.20	2.8	1.3	3.8	3.9	4.4	4.0	3.51	3.7
Tb	1.0	0.75	0.90	0.4	0.2	0.6	0.7	0.7	0.6	0.61	0.5
Dy	4.9	4.36	5.03	1.9	0.8	3.1	3.2	3.2	3.2	3.54	2.6
Ho	1.1	0.86	0.98	0.4	0.2	0.7	0.8	0.8	0.8	0.71	0.6
Er	2.5	2.46	2.85	1.0	0.4	1.9	2.1	1.9	1.9	2.02	1.6
Tm	0.31	0.363	0.408	0.14	0.07	0.29	0.30	0.29	0.31	0.315	0.22
Yb	1.60	2.24	2.51	0.90	0.30	1.90	1.80	1.7	1.80	1.88	1.40
Lu	0.24	0.335	0.379	0.13	0.07	0.27	0.31	0.26	0.28	0.282	0.23
Hf	1.7	3.0	6.0	4.2	2.3	4.5	7.5	3.8	3.2	4.2	4.9
Ta	1.67	0.09	<0.01	1.13	0.74	0.91	1.44	0.64	0.91	<0.01	1.00
Tl	<0.1	0.14	0.53	0.2	0.2	0.2	0.3	0.3	0.2	0.37	0.2
Pb	4	5	20	7	2	9	14	10	7	18	13
Th	0.50	3.78	9.05	5.77	2.92	4.94	7.52	3.19	5.09	8.26	2.90
U	0.35	0.74	2.45	1.95	1.14	1.62	1.66	1.14	1.32	1.42	1.03
Eree	116.5	95.7	147.5	117.7	53.6	108.5	128.3	114.4	99.9	113.4	122.8
La_N/yb_N	6.71	4.97	8.10	20.85	29.77	8.09	10.62	8.72	7.54	8.47	13.11
Eu/Eu*	1.32	0.95	0.66	0.93	1.19	0.89	0.84	0.83	0.91	0.79	0.94
Sri											

Note: Analyses by Actlabs by ICP-optical (major oxides) and mass spectrometry (trace elements) and XRF (as noted).

(continued)

TABLE 3. CHEMICAL ANALYSES OF GRANITIC ROCKS, SINALOA BATHOLITH *(continued)*

	Posttectonic rocks										
Unit:	San Ignacio granodiorite								El Carmen granodiorite	Concordia granodiorite	
Sample:	HP-1	HS-40	HS-41	HS-42	HP-11	156	146	HP-26	HS-25	HS-8B	HS-19
Map unit:	TKis	TKis	TKis	TKis	TKis	TKis	TKis	TKis	TKie	TKicn	TKicn?
SiO_2	62.84	66.92	54.94	66.41	66.44	64.32	63.30	65.14	66.73	65.13	58.10
TiO_2	0.78	0.57	0.96	0.64	0.61	0.68	0.76	0.67	0.52	0.60	0.77
Al_2O_3	16.13	15.96	21.28	14.92	15.17	15.06	15.91	15.97	15.65	16.22	17.49
Fe_2O_3	1.21	1.98	3.67	4.54	0.66	5.96	5.47	1.50	1.11	0.67	2.62
FeO*	4.96	2.56	2.83		4.01			3.21	3.29	3.66	4.85
MnO	0.11	0.06	0.08	0.07	0.08	0.10	0.08	0.08	0.09	0.08	0.14
MgO	2.53	1.93	2.58	1.85	1.95	2.16	2.44	2.04	2.02	2.29	3.94
CaO	4.92	4.73	7.15	3.81	3.95	4.42	5.01	4.30	4.40	4.73	7.01
Na_2O	3.02	3.45	4.19	3.08	3.20	3.21	3.39	3.58	3.49	3.57	3.24
K_2O	3.34	1.67	1.99	3.80	3.79	3.48	2.84	3.36	2.55	2.91	1.64
P_2O_5	0.15	0.16	0.35	0.12	0.13	0.13	0.17	0.15	0.15	0.14	0.19
H_2O+											
H_2O-											
LOI	0.39	1.05	1.08	0.33	0.45	0.78	0.92	0.74	1.56	1.29	1.59
Total*	100.39	101.05	101.08	99.58	100.45	100.31	100.28	100.74	101.56	101.29	101.59
Sc xrf	19	5	6	13	12	14	13	11	12	16	22
V	181	82	79	94	82	128	114	106	95	103	168
Ni	26	44	13	<20	16	<20	<20	21	5	25	23
Cu	50	<5	53	25	75	40	29	39	24	13	8
Zn	66	77	97	-30	57	72	74	83	62	110	104
Ga	17	18	21	16	12	17	20	19	17	18	19
As	9	<5	44	<5	5	<5	<5	9	<5	7	<5
Rb	139	49	54	172	140	149	147	190	81	154	48
Sr	330	650	884	273	211	270	385	381	403	443	511
Sr xrf	316	638	940	269	262	269	379	364	389	430	479
Y	24	6	8	23.9	18	24.0	22.6	23	13	22	16
Y xrf	24	6	9	23.0	23	23.0	22.0	23	13	22	16
Zr	251	143	320	227	141	203	202	213	105	187	91
Zr xrf	255	154	362	232	181	213	198	223	104	206	90
Nb	10.5	4.6	6.3	6.7	6.7	15.3	9.0	11.1	6.5	9.2	4.9
Mo	7.4	6.0	4.4	<2	5.4	7	2	14.2	7.6	9.2	5.2
Sb	2.4	<0.1	1.8	0.4	6.1	0.6	0.3	1.7	0.3	1.2	0.6
Cs	5.8	2.2	2.9	7.5	5.2	9.0	7.2	9.2	3.8	4.2	2.5
Ba	827	926	1075	816	573	862	708	732	877	824	641
Ba xrf	837	937	1192	795	761	836	675	747	887	827	631
La	24.3	12.1	18.2	20.7	26.9	25.8	27.1	39.7	24.2	21.5	14.2
Ce	49.5	21.3	32.1	45.3	51.8	53.6	57.2	77.6	43.0	47.4	29.7
Pr	5.86	2.28	3.53	5.52	5.62	6.21	6.67	8.51	4.68	5.83	3.58
Nd	22.3	8.7	12.7	21.5	20.0	23.8	25.2	30.4	16.1	23.7	14.9
Sm	4.9	1.6	2.3	4.70	3.9	4.94	5.14	5.9	3.0	5.0	3.3
Eu	1.15	0.79	1.08	0.864	0.74	0.944	1.09	1.11	0.79	0.98	1.00
Gd	4.8	1.2	1.9	4.03	3.5	4.23	4.21	5.0	2.6	4.1	3.2
Tb	0.8	0.2	0.3	0.71	0.6	0.74	0.71	0.8	0.4	0.8	0.5
Dy	4.1	1.0	1.3	4.06	2.9	4.17	3.90	4.0	2.0	3.5	2.8
Ho	1.0	0.2	0.3	0.80	0.7	0.80	0.73	0.9	0.5	0.9	0.7
Er	2.5	0.6	0.8	2.32	1.8	2.32	2.07	2.3	1.3	2.3	1.8
Tm	0.39	0.10	0.14	0.356	0.27	0.356	0.303	0.35	0.20	0.35	0.28
Yb	2.4	0.70	0.90	2.17	1.7	2.19	1.93	2.2	1.30	2.30	1.70
Lu	0.35	0.11	0.17	0.330	0.25	0.326	0.283	0.31	0.20	0.33	0.28
Hf	7.0	4.0	7.1	6.4	4.0	5.7	5.3	6.1	3.0	5.4	2.6
Ta	0.90	1.09	0.70	0.91	0.71	11.4	2.62	1.28	1.44	2.03	0.73
Tl	0.4	0.3	0.3	0.69	1.8	0.82	0.79	0.9	0.4	0.5	0.3
Pb	10	10	8	12	205	31	20	19	11	9	9
Th	16.08	2.94	3.79	19.4	17.88	24.3	24.8	30.28	8.25	18.32	2.88
U	4.83	1.51	1.87	4.62	4.37	6.22	6.71	9.28	1.82	6.51	0.87
Eree	124.4	50.9	75.7	113.3	120.7	130.4	136.6	179.1	100.3	119.0	77.9
La_N/yb_N	7.01	11.97	14.00	6.60	10.96	8.17	9.73	12.49	12.89	6.47	5.78
Eu/Eu*	0.71	1.66	1.52	0.59	0.60	0.61	0.69	0.60	0.84	0.64	0.92
Sri				0.7030		0.7062		0.7058			

Note: Analyses by Actlabs by ICP-optical (major oxides) and mass spectrometry (trace elements) and XRF (as noted).

(continued)

TABLE 3. CHEMICAL ANALYSES OF GRANITIC ROCKS, SINALOA BATHOLITH *(continued)*

	Posttectonic rocks										
Unit:	Candelero granodiorite										
Sample:	HP-6	HP-13	236	HP-25	HP-28	HP-23	HC-3	HS-49	HS-50	HS-15	HS-23
Map unit:	TKica	TKica	Tkica	TKica	TKica	TKica	Tkica	TKi	TKi	Tki	Tki
SiO_2	63.86	71.70	70.48	65.22	68.90	67.47	66.84	63.63	62.96	61.86	67.05
TiO_2	0.65	0.36	0.31	0.71	0.50	0.62	0.49	0.69	0.60	0.82	0.54
Al_2O_3	16.30	14.08	14.29	16.76	15.39	15.64	16.35	16.16	16.96	16.60	15.56
Fe_2O_3	1.02	0.11	3.05	0.94	0.71	3.85	1.10	2.73	2.29	1.98	1.25
FeO*	4.48	2.92		3.29	2.43		2.83	2.87	3.26	4.13	2.88
MnO	0.10	0.06	0.06	0.07	0.04	0.06	0.07	0.09	0.10	0.10	0.08
MgO	2.41	0.88	1.11	1.67	1.23	1.16	1.62	2.58	2.52	2.80	1.99
CaO	4.86	2.49	2.94	4.59	3.33	3.73	4.14	4.87	5.55	5.42	4.18
Na_2O	3.73	3.20	3.23	4.21	3.80	4.14	4.29	3.36	3.67	3.47	3.49
K_2O	2.40	4.11	3.95	2.32	3.54	2.74	2.11	2.85	1.90	2.63	2.83
P_2O_5	0.18	0.10	0.08	0.21	0.13	0.20	0.16	0.16	0.19	0.18	0.14
H_2O+											
H_2O-											
LOI	0.58	0.29	0.76	0.44	0.35	0.65	0.54	1.49	1.41	1.40	1.05
Total*	100.58	100.29	100.25	100.44	100.35	100.27	100.54	101.49	101.41	101.40	101.05
Sc xrf	11	5	7	6	6	6	8	18	16	18	13
V	133	61	60	94	65	73	82	127	114	136	88
Ni	21	21	<20	18	18	<20	16	18	8	37	17
Cu	17	15	<10	9	9	16	17	28	13	45	27
Zn	78	46	34	77	51	66	47	90	90	798	62
Ga	18	17	14	20	18	22	19	18	18	18	16
As	<5	<5	<5	<5	<5	<5	<5	7	<5	8	47
Rb	74	165	149	79	135	86	50	120	57	119	108
Sr	488	226	236	545	367	508	514	380	523	390	354
Sr xrf	464	217	239	541	360	507	505	369	514	376	341
Y	15	13	10.8	11	11	12.2	9	22	15	21	16
Y xrf	15	13	12.0	12	12	12.0	10	22	16	22	16
Zr	149	125	109	148	129	159	102	165	128	165	126
Zr xrf	145	118	99	150	140	159	101	171	128	181	142
Nb	8.4	7.2	6.8	7.3	5.5	9.6	7.2	8.8	6.8	10.1	6.9
Mo	8.4	20.7	2	7.4	7.7	2	8.2	10.8	7.3	7.5	7.4
Sb	1.7	1.4	0.2	1.1	1.0	<0.2	3.3	0.6	0.4	8.8	2.1
Cs	2.5	4.6	4.5	2.7	3.3	1.5	2.2	6.6	2.3	6.6	4.3
Ba	952	672	729	720	713	926	807	778	954	683	904
Ba xrf	976	679	711	760	745	884	823	796	957	701	927
La	27.1	30.3	13.0	22.7	22.1	28.6	21.3	38.2	21.3	23.0	18.9
Ce	50.6	59.1	25.6	46.0	42.2	58.1	39.4	74.8	41.4	47.7	36.9
Pr	5.56	6.31	2.82	5.38	4.79	6.72	4.27	8.17	4.89	5.62	4.31
Nd	20.4	22.2	10.1	21.0	17.7	25.2	15.3	29.6	18.1	21.6	16.2
Sm	3.9	4.0	1.84	4.2	3.4	4.60	2.8	5.4	3.6	4.4	3.4
Eu	1.07	0.81	0.533	1.16	0.86	1.22	0.84	0.99	1.08	1.11	0.89
Gd	3.4	3.2	1.64	3.4	2.9	3.36	2.4	4.7	3.0	4.4	3.1
Tb	0.5	0.5	0.28	0.5	0.4	0.47	0.3	0.7	0.5	0.7	0.5
Dy	2.5	2.2	1.64	2.1	2.0	2.29	1.6	3.7	2.6	3.7	2.6
Ho	0.6	0.5	0.34	0.4	0.4	0.40	0.4	0.9	0.6	0.9	0.6
Er	1.5	1.2	1.02	1.0	1.0	1.07	0.9	2.3	1.7	2.2	1.6
Tm	0.24	0.19	0.169	0.14	0.15	0.151	0.14	0.34	0.25	0.35	0.26
Yb	1.6	1.2	1.15	0.9	0.90	0.95	1.0	2.20	1.70	2.20	1.60
Lu	0.23	0.17	0.195	0.13	0.15	0.140	0.14	0.32	0.26	0.34	0.25
Hf	4.2	3.7	3.2	4.2	3.9	4.3	2.9	4.9	3.5	4.6	3.6
Ta	0.87	0.75	2.86	0.60	0.65	5.49	0.89	1.67	0.92	1.66	2.18
Tl	0.4	0.9	0.74	0.3	0.6	0.45	0.2	0.6	0.3	0.6	0.5
Pb	13	14	22	8	10	24	8	14	12	86	11
Th	8.73	36.15	38.0	10.53	25.87	15.2	6.21	12.98	4.98	16.05	11.13
U	2.89	8.61	12.4	3.20	6.31	3.11	2.20	4.71	1.55	4.02	3.89
Eree	119.2	131.9	60.4	109.0	99.0	133.3	90.8	172.3	101.0	118.2	91.1
La_N/yb_N	11.73	17.48	7.87	17.46	17.00	20.94	14.75	12.02	8.67	7.24	8.18
Eu/Eu*	0.87	0.67	0.91	0.90	0.81	0.90	0.96	0.58	0.97	0.76	0.82
Sri		0.7050			0.7044						

Note: Analyses by Actlabs by ICP-optical (major oxides) and mass spectrometry (trace elements) and XRF (as noted).

(continued)

TABLE 3. CHEMICAL ANALYSES OF GRANITIC ROCKS, SINALOA BATHOLITH *(continued)*

	Posttectonic rocks								
Unit:									Colegio tonalite
Sample:	HM-9	HP-16	HP-5	HP-7	199	HS-52	HP-17	HP-22	HS-53
Map unit:	Tki	Tki	Tki	TKi	Tki	TKi	TKi	TKi	Tic
SiO_2	74.16	65.96	64.91	53.81	57.39	58.68	67.22	63.25	60.88
TiO_2	0.12	0.63	0.67	0.73	0.94	0.97	0.59	0.80	0.81
Al_2O_3	13.70	14.92	15.51	21.41	16.92	16.47	14.91	15.73	16.72
Fe_2O_3	<0.01	5.08	5.11	1.58	7.84	3.76	0.31	5.51	6.24
FeO*	2.54			4.51		3.10	4.45		
MnO	0.06	0.08	0.08	0.09	0.12	0.11	0.08	0.09	0.12
MgO	0.37	2.12	2.12	3.66	3.72	4.06	1.78	2.70	2.77
CaO	1.10	4.34	4.63	9.33	6.85	6.51	3.85	5.17	5.52
Na_2O	3.84	3.12	3.56	3.05	3.29	3.54	3.10	3.25	4.13
K_2O	4.04	3.32	2.93	1.72	1.61	2.54	3.59	2.92	2.06
P_2O_5	0.07	0.13	0.14	0.11	0.21	0.25	0.12	0.18	0.22
H_2O+									
H_2O-									
LOI	0.45	0.44	0.60	1.35	0.95	1.53	0.50	0.63	0.41
Total*	100.45	100.13	100.26	101.35	99.83	101.53	100.50	100.21	99.87
Sc xrf	4	13	13	18	18	22	11	15	14
V	44	120	133	184	175	171	143	113	128
Ni	29	<20	<20	34	<20	33	25	<20	<20
Cu	11	12	25	181	20	59	15	33	11
Zn	44	60	33	79	-30	121	55	80	79
Ga	18	18	18	20	15	19	17	19	19
As	<5	<5	9	13	<5	10	7	<5	<5
Rb	140	132	110	98	64	78	149	141	80
Sr	162	284	362	560	428	564	282	373	451
Sr xrf	157	278	357	536	441	541	265	377	453
Y	21	26.4	21.6	13	23.3	21	24	24.0	18.5
Y xrf	19	26.0	21.0	13	22.0	21	23	25.0	18.0
Zr	61	149	173	90	157	220	183	200	111
Zr xrf	64	154	167	95	162	204	160	213	115
Nb	7.6	5.9	6.0	5.4	6.7	9.7	8.5	6.4	6.1
Mo	8.9	4	3	6.1	2	6.6	11.6	4	<2
Sb	2.1	0.5	0.8	4.3	-0.2	1.0	1.6	0.4	0.2
Cs	3.5	4.3	5.2	14.1	3.1	1.6	5.9	5.2	3.2
Ba	716	748	857	358	633	677	873	710	634
Ba xrf	714	727	813	358	628	678	875	691	615
La	18.0	31.0	27.6	14.9	22.8	25.6	24.4	24.8	22.3
Ce	34.7	61.7	56.8	29.0	47.1	53.6	48.8	54.3	43.8
Pr	3.86	6.91	6.60	3.25	5.63	6.51	5.66	6.68	5.09
Nd	13.4	25.4	24.7	12.2	22.4	25.5	21.6	26.3	19.9
Sm	3.1	5.11	4.90	2.7	4.76	5.1	4.6	5.46	3.86
Eu	0.47	0.999	0.955	0.89	1.29	1.29	1.05	1.09	1.13
Gd	3.1	4.36	4.06	2.6	4.12	4.9	4.5	4.55	3.26
Tb	0.6	0.76	0.67	0.4	0.72	0.7	0.7	0.77	0.56
Dy	3.3	4.39	3.71	2.2	4.06	3.6	3.7	4.25	3.15
Ho	0.8	0.87	0.72	0.5	0.79	0.9	0.9	0.79	0.64
Er	2.1	2.46	2.05	1.2	2.18	2.3	2.4	2.27	1.89
Tm	0.34	0.375	0.312	0.21	0.316	0.34	0.36	0.328	0.283
Yb	2.1	2.39	1.92	1.2	1.98	2.10	2.4	2.05	1.84
Lu	0.31	0.355	0.289	0.18	0.284	0.33	0.34	0.308	0.279
Hf	2.2	4.6	4.6	2.7	3.6	6.1	5.2	5.5	3.5
Ta	1.08	<0.01	<0.01	0.45	<0.01	1.10	1.15	<0.01	<0.01
Tl	0.8	0.76	0.38	1.1	0.16	0.3	0.7	0.75	0.51
Pb	21	24	12	12	<5	9	11	21	24
Th	7.85	18.2	23.3	5.57	8.88	9.41	12.98	21.9	8.69
U	4.18	5.11	5.16	1.65	2.21	2.82	4.84	6.46	2.51
Eree	86.2	147.2	135.3	71.4	118.5	132.8	121.4	133.9	107.9
La_N/yb_N	5.93	8.99	9.95	8.60	7.99	8.44	7.04	8.38	8.42
Eu/Eu*	0.46	0.63	0.63	1.01	0.87	0.77	0.69	0.65	0.94
Sri									

Note: Analyses by Actlabs by ICP-optical (major oxides) and mass spectrometry (trace elements) and XRF (as noted).

al., 1982; Henry and Fredrikson, 1987; Clarke and Titley, 1988; Staude and Barton, 2001). These data indicate that posttectonic intrusions were emplaced at depths less than 3 km.

Interpretation of K-Ar results for the syn- or pretectonic intrusions is not so straightforward. Only three of nine syntectonic pairs are concordant, and the larger absolute age difference allowed by concordance for them does not preclude slow cooling. Syntectonic granites intrude Jurassic(?) metasedimentary rocks. A few amphibolite outcrops of uncertain protolith are the only possible volcanic equivalent. The syntectonic rocks were probably emplaced at greater depths than were posttectonic rocks, although how deep is unknown. Moreover, the syntectonic rocks show common evidence of deformation at moderate temperatures during or following emplacement.

The small absolute differences between U-Pb and K-Ar ages are nearly constant in percentage, but they may still reflect geologic environments. The 20 Ma Colegio granodiorite (HS-53) probably was emplaced into the coolest environment, as no other dated plutons of that age have been recognized. The 48 Ma Candelero and 67 Ma San Ignacio granodiorites were emplaced during a period of intense and repeated batholithic intrusion, and thus presumably into a much hotter environment; their larger absolute age differences could reflect this. Finally, the 101 Ma Recodo tonalite was also emplaced during repeated granitic intrusion and possibly at greater depth and has the largest absolute difference between K-Ar and U-Pb ages.

A further observation is that the biotite age in some discordant samples is indistinguishable from the concordant age of a younger, adjacent intrusion, whereas the hornblende age appears unaffected. This is best illustrated by three samples of the El Carmen granodiorite in the north-central part of the map area (Fig. 2). Sample HS-12, which was collected at least 6 km from the nearest younger intrusion, has concordant biotite (75.0 ± 0.8 Ma) and hornblende (73.0 ± 1.6 Ma) ages. Biotite in two other samples is significantly younger. Biotite in sample HS-13 gives 62.9 ± 0.7 Ma, which is indistinguishable from numerous ages for the nearby San Ignacio granodiorite. Hornblende in HS-13 gives 74.7 ± 1.7 Ma, indistinguishable from the concordant age of HS-12, which suggests it lost no measurable Ar despite reheating that completely reset biotite. Similarly, biotite in sample HS-25 gives 65.2 ± 0.7 Ma, whereas hornblende is 73.4 ± 1.6 Ma. No other dated rock lies near sample HS-25, so it is not possible to determine whether the biotite age has been completely reset. Nevertheless, the hornblende has again been unaffected.

The 52.7 Ma biotite age of the 101 Ma sample HS-17 is also indistinguishable from the concordant ages of an adjacent pluton. Sample HS-8B of the Concordia granodiorite gives 53.8 ± 0.6 (biotite) and 54.2 ± 1.2 Ma (hornblende). Although sample HS-8B was collected ~17 km to the southeast, we traced the Concordia pluton to within 6 km of sample HS-17. Notably, neither biotite nor hornblende in sample HM-4, which is farther from the Concordia intrusion, appears affected.

Finally, sample 146 was collected from within what appears to be a 1-km-diameter inclusion of San Ignacio granodiorite in Candelero granodiorite and no more than 100 m from the contact. The biotite age of 146 (47.0 ± 0.5 Ma) has been reset to the concordant age of the Candelero intrusion. Assuming the San Ignacio body was emplaced at ca. 64 Ma, the hornblende age of 49.6 ± 1.1 Ma suggests it has been only partly reset.

A reasonable interpretation of these data is that biotites were completely reset by intrusion of the younger plutons, but that hornblendes were generally unaffected. Discordance appears to be solely the result of reheating by younger plutons, not of slow cooling of any origin. Therefore, hornblende ages, even in discordant samples, indicate the time of emplacement. As with our interpretation of concordant data, this interpretation is most straightforward for the posttectonic intrusions.

An alternative interpretation, that the concordant ages represent rapid uplift long after emplacement, seems impossible. Samples with concordant ages range from 98 to 20 Ma. This alternative would require a checkerboard of small uplifts, on the order of 10^2 km^2, throughout that time while adjacent areas remained at depth. This situation is in marked contrast to that in the Peninsular Ranges batholith, where regional uplift long after intrusion has exposed deep levels of the eastern part of the batholith and generated a regional pattern of generally discordant K-Ar dates that are variably younger than U-Pb zircon ages (Gastil, 1975; Krummenacher et al., 1975; Silver et al., 1979; Silver and Chappell, 1988; Snee et al., 1994; Ortega-Rivera et al., 1997; Ortega-Rivera, this volume, Chapter 11).

PRE-BATHOLITHIC ROCKS

Pre-batholithic rocks include quartz diorite orthogneiss and metasedimentary and metavolcanic(?) rocks. Orthogneiss crops out in two small areas in the south-central part of the map area, where it is in contact with both metamorphosed sandstone and early gabbro of the batholith (Fig. 2, Plate 1). Gneiss in the eastern area 26 km northeast of Mazatlan contains quartz, plagioclase, biotite, hornblende, and minor orthoclase. Metamorphism has produced aligned aggregates of biotite and hornblende and mosaics of strained quartz. Foliation strikes N 40° E and dips steeply northwest, concordant with bedding and schistosity in the metasedimentary rocks (Plate 1). Strongly foliated granitic gneiss is exposed ~30 km north of Mazatlan west of Highway 15. The gneiss is cut by many tabular amphibolite bodies, possibly metamorphosed diabase dikes. Foliation and axes of recumbent folds in the gneiss and amphibolite strike irregularly northwest. This early granitic magmatism is distinguished from the main batholith by the strong metamorphic overprint and a possible Jurassic age. Similar metamorphosed granitic rocks are recognized in northern Sinaloa (Mullan, 1978). Anderson et al. (1972) and Damon et al. (1984) identified a Jurassic (190–160 Ma) magmatic arc that extends the length of México; gneiss in Sinaloa may be part of this arc.

Two sequences of metasedimentary rocks crop out in southern Sinaloa. The most extensive consists of phyllitic sandstone, quartzite, and quartz-biotite-muscovite schist (Jm). Protolith was

finely laminated to massive muddy sandstone and siltstone. Detrital grains are mostly quartz with lesser chert and plagioclase. Marble and minor quartz-, garnet-, and epidote-bearing calc-silicate rock (Kl) form an east-trending belt 30 km north of Mazatlan (Fig. 2, Plate 1). The metamorphosed clastic rocks and marble generally do not occur together. Nevertheless, bedding and schistosity in both are parallel and strike east to east-northeast, suggesting they have undergone the same deformation. Amphibolite was found in scattered locations, some adjacent to marble, but its protolith is uncertain. The amphibolite could be in part metamorphosed mafic to intermediate volcanic rock, which in turn could be volcanic equivalents of some early batholithic rocks.

The metamorphosed clastic rocks are probably Jurassic, and the marble is almost certainly Aptian. Similar metamorphic rocks of the El Fuerte Group in northern Sinaloa are Jurassic or older (Mullan, 1978), and slightly metamorphosed graywackes and argillites, the oldest known rocks in Nayarit, are thought to be Late Jurassic (Gastil et al., 1978). Holguin (1978) and Bonneau (1970) demonstrated that metamorphosed carbonate rocks throughout Sinaloa are early Aptian (ca. 113–110 Ma), which precedes emplacement of the main batholith. Bonneau also found andesite, conglomerate, limestone, and dolomite underlying the marble in central Sinaloa. Amphibolite in southern Sinaloa could be equivalent to the andesite found by Bonneau.

THE SINALOA BATHOLITH

Intrusive rocks of the Sinaloa batholith crop out over much of the region west of the Sierra Madre Occidental (Figs. 1 and 2, Plate 1). In our Sinaloa map area, more than a third of outcrop is granitic; the rest of the outcrop is mostly younger cover. Batholiths are exposed in all the deeply incised canyons of the Sierra Madre, so they are probably extensive beneath it. Therefore, batholithic rocks probably underlie most of the region.

Granodiorite is the most abundant rock, but compositions of individual intrusions range from gabbro to granite (Figs. 4 and 5, Appendix 2). Plagioclase, quartz, alkali feldspar, biotite, hornblende, and clinopyroxene are major phases. Sphene is a common accessory, and large euhedral grains are particularly prominent in some posttectonic rocks. Other accessory minerals, present in most samples, are zircon, apatite, and epidote.

The Sinaloa batholith developed in three stages. Early gabbros may have been emplaced ca. 135 Ma. Foliated pre- or syntectonic rocks were emplaced before ca. 90 Ma, apparently while the region was being deformed and are mostly tonalites. Posttectonic rocks were emplaced between ca. 90 and 45 Ma, with one intrusion at 20 Ma, and after deformation had ceased; they are predominantly granodiorite.

Early Gabbro

Gabbro crops out as two tabular, east-northeast–striking bodies that intrude the clastic metasedimentary rocks (Fig. 2, Plate 1). A western body, ~7 km by 12 km, crops out in roadcuts along Highway 15, 20 km north of Mazatlan. An eastern body, ~7 km by 4 km, is well exposed in roadcuts along the paved road to La Noria, 20 km northeast of Mazatlan and ~8 km south of La Noria. A small, unmapped quartz-bearing gabbro (HS-48) crops out within granitic rocks ~10 km east of the eastern body. Cumulus layering in the two main bodies generally strikes east-northeast and dips northwest parallel to contacts, bedding, and schistosity in the enclosing metasedimentary rocks. Marble appears to be in depositional contact on the western gabbro in a quarry off Highway 15.

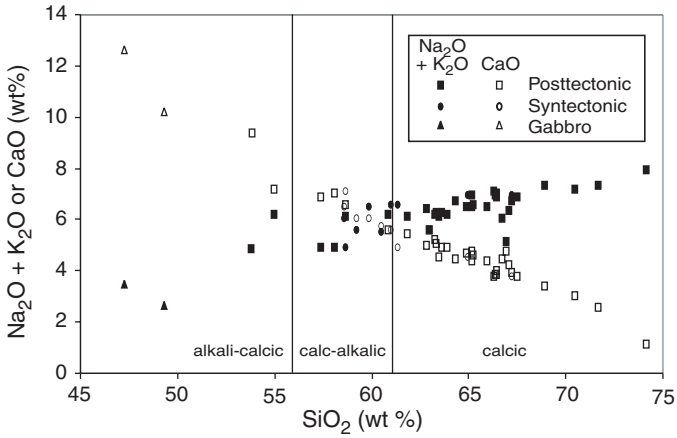

Figure 4. Plot of weight % Na_2O + K_2O and CaO versus SiO_2 for chemical analyses of Sinaloa batholith, which is borderline calc-alkalic or calcic.

Plagioclase-clinopyroxene ± hornblende gabbro is the dominant rock type in both bodies, but pyroxenite and anorthosite are also present. The rocks are variably altered or metamorphosed. Plagioclase is commonly bent and shows minor sericitic alteration. Pyroxene locally contains cores of a colorless, fibrous amphibole, probably tremolite, and is rimmed by hornblende. Mafic minerals are locally replaced by actinolite.

Hornblendes from the eastern intrusion and from the unmapped quartz-bearing gabbro give similar K-Ar ages of 133.8 ± 3.0 (HS-46) and 138.6 ± 3.1 (HS-48). These ages could indicate the time of emplacement, excess Ar, or cooling following metamorphism. If marble is early Aptian and depositionally on gabbro, then the gabbro is at least ca. 110 Ma. Given the resistance of hornblende to Ar loss and the improbability that metamorphism reached 500 °C, the ages are not likely to reflect cooling following metamorphism. Because the amphiboles have very different K contents (~0.15 and 0.42) but similar ages, excess Ar would have had to have been incorporated proportional to their K contents. Excess Ar has been interpreted for similar gabbros of the Peninsular Ranges, which give hornblende K-Ar ages as old as 146 Ma (Krummenacher et al., 1975), because no U-Pb ages are that old (Silver et al., 1979). Similar metamorphosed mafic intrusions are present in northern Sinaloa but are not dated (Mullan, 1978; Ortega-Gutiérrez et al., 1979).

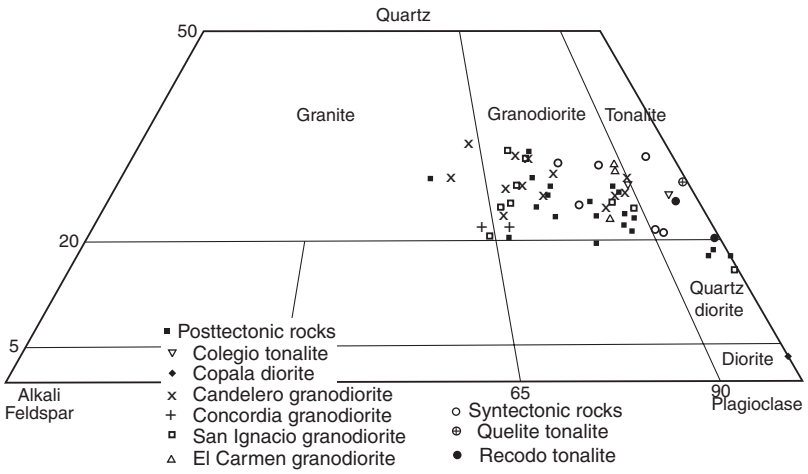

Figure 5. Quartz-alkali feldspar-plagioclase modes of granitic rocks of Sinaloa batholith. Syntectonic rocks are relatively mafic tonalites and granodiorites containing 15–28% mafic minerals. Posttectonic rocks are mostly more leucocratic granodiorites and lesser granite containing 5–20% mafic minerals; minor posttectonic quartz diorites are border phases or small intrusions. The 20 Ma Colegio tonalite, which contains 24% mafic minerals, is compositionally like the pre–90 Ma syntectonic rocks and crops out in same location near coast.

Syntectonic Intrusions

A group of tonalites to mafic granodiorites commonly showing evidence of deformation during or following emplacement are at least 90 Ma based on both K-Ar and U-Pb dates. These pre- or syntectonic intrusions are distinctly more mafic than later, posttectonic intrusions (up to 28 modal percent mafic minerals; Fig. 5) and contain lesser potassium feldspar, which is mostly microcline. For simplicity, we refer to these rocks as syntectonic, although whether they intruded during or before deformation is unknown.

All known syntectonic rocks crop out within 50 km of the coast, both in the map area and in northern Sinaloa (Figs. 1 and 2, Plate 1); they are the dominant intrusive type within ~25 km. Individual plutons are probably no more than 8 km in diameter, as individual rock types cannot be traced more than that distance. Two distinctive plutons have been mapped separately. A strongly foliated, mafic, coarse-grained tonalite (Quelite tonalite; Kiq) crops out ~35 km north of Mazatlan. A fine-grained, non-foliated tonalite ~25 km northeast of Mazatlan (Recodo tonalite; Kir; dated at 101 Ma by U-Pb) contains 25–28% mafic minerals and minor microcline. Quartz occurs as poikilitic grains enclosing plagioclase, biotite, and hornblende. Hornblende surrounds cores of augite and tremolite(?). Foliation in the Quelite tonalite (Kiq) strikes east-northeast, is vertical, and is approximately parallel to foliation in enclosing marble. The orientation of foliation in other syntectonic rocks is unknown because the foliation is generally faint and because most outcrops in the coastal plain consist of large residual boulders that are not strictly in place.

Most syntectonic rocks are weakly foliated and show varying degrees of dynamic recrystallization. The most common texture is recrystallization or subgrain development of quartz, which is strongly to weakly developed in different samples. In rocks showing the greatest quartz recrystallization, a few plagioclase grains are cut by through-going fractures and filled with quartz. A few plagioclase grains in the same rock are bent, but we see little or no evidence of subgrain development in plagioclase. In less deformed rocks, interstitial microcline shows undulatory extinction, suggesting incipient recrystallization. Myrmekite is common at microcline-plagioclase boundaries; although locally present in posttectonic rocks, this texture is far more common in syntectonic rocks and may be an indicator of deformation (Vernon, 1991). Dynamic recrystallization textures are most intense in samples HS-34, HS-44, HS-45, and HS-37 near the coast, less intense in samples HS-22 and HM-8 to the east, and absent in the Recodo tonalite samples farther south (HS-17 and HM-4). The petrographic characteristics suggest deformation occurred above 300 °C, the temperature required for dynamic recrystallization of quartz, but probably below 450 °C, the minimum temperature of plagioclase recrystallization (Tullis, 1983).

Timing of emplacement for these rocks is anchored by the U-Pb age of Recodo tonalite (HS-17; 101.2 ± 2.0 Ma) and concordant K-Ar dates on sample HM-4 (biotite: 98.3 ± 1.1 Ma; hornblende 96.3 ± 2.2) from the same pluton. However, the time of emplacement of other syntectonic rocks and of the end of deformation are not fully understood. Only two other samples are concordant (HC-4A, biotite 92.1 ± 1.0, hornblende, 90.4 ± 2.0; HC-5, biotite 88.6 ± 1.0, hornblende 89.5 ± 2.0 Ma), and both of these are from the northern Sinaloa transect. All other samples are discordant, with hornblende ages slightly to 27 Ma greater than biotite ages (Table 1); hornblende from sample HS-34 is 3.3 Ma less than the biotite age of 89.8 Ma. Notably, neither of the two samples of Recodo tonalite show evidence of deformation. Sample HC-4A and all other dated syntectonic samples show hand specimen and petrographic evidence of deformation, and their hornblende ages range from 97.9 ± 2.2 Ma (HS-22) to 86.5 ± 1.9 Ma (HS-34).

These observations imply that either (1) all the deformed intrusions are older than 101 Ma and neither concordant nor hornblende ages of the syntectonic rocks record time of emplacement, or (2) the Recodo tonalite was emplaced before or during deformation but remained undeformed. The latter is possible, because deformation could have been concentrated in narrow

zones with intervening areas showing less or no deformation. The syntectonic rocks can be no older than ca. 110 Ma, the approximate age of Aptian marble that they intrude.

For all deformed intrusions to be older than 101 Ma, they would have to have been maintained at temperatures greater than ~500 °C until the maximum apparent hornblende age of 97.9 ± 2.2 Ma (HS-22), i.e., any regional cooling must have been ≤98 Ma. The ca. 98 Ma concordant ages of sample HM-4 require the same conditions. However, the irregular pattern of hornblende (as well as biotite) ages demonstrates they are not all recording the same regional cooling. The younger hornblende ages could reflect variable reheating by later plutons, yet the data of sample 146 suggest that such reheating is only able to reset hornblende if the younger pluton is closer than 100 m. Therefore, it seems more likely that they do indicate time of emplacement. These uncertainties leave open the question as to when deformation recorded by the syntectonic plutons occurred or ended. Additional U-Pb as well as $^{40}Ar/^{39}Ar$ dating is needed.

Posttectonic Intrusions

Most intrusions lack foliation or dynamic recrystallization textures and were emplaced after any observable deformation ended. Their ages in the main map area range from ca. 82 to 45 Ma, with one intrusion at 20 Ma. Where observed, contacts indicate that posttectonic rocks cut syntectonic rocks. These posttectonic intrusions range from diorite to monzogranite but are predominantly granodiorite and distinctly less mafic than the syntectonic rocks. Potassium feldspar, which is orthoclase in all samples, and quartz are more abundant than in the syntectonic rocks (Fig. 5), and mafic minerals make up no more than 15 modal percent. Posttectonic rocks are widely distributed throughout the map area from within ~12 km of the coast, where they intrude syntectonic rocks and metasedimentary rocks, to the Sierra Madre Occidental, where they crop out in the deep canyons of the Rio Piaxtla and Rio Presidio (Plate 1) and intrude the lower volcanic complex. Posttectonic intrusions also crop out along the transect in northern Sinaloa, where they are as old as 89 Ma.

Posttectonic intrusions are generally larger than syntectonic intrusions and reach dimensions of 15 km north-south and up to 25 km east-west. However, these latter dimensions are parallel to extension that affected southern Sinaloa and a large region surrounding the Gulf of California (Henry, 1989; Stock and Hodges, 1989; Henry and Aranda-Gómez, 2000). Their true, unextended east-west dimensions are probably closer to 15 km also.

Six posttectonic rock types have been mapped separately, but only two are sufficiently distinctive and widespread to be correlated beyond individual plutons. The Candelero granodiorite (TKic) is named for exposures in the Arroyo de Candelero in the northeastern part of the map area (HP-14; Fig. 2). It forms several plutons across the northern part as well as one cutting syntectonic rocks 20 km north of Mazatlan (Fig. 2, Plate 1). The Candelero granodiorite is medium grained and distinguished by 5–10% large euhedral biotite and hornblende. Euhedral sphene to 2 mm is common. Field relations indicate that the Candelero is the youngest major intrusive phase. Similar rocks crop out ~20 km north of the northwest corner of Figure 2 and 200 km to the northwest along our northern transect (HC-3; Fig. 1). Furthermore, the Candelero granodiorite is petrographically similar to the La Posta type of the Peninsular Ranges batholith and Los Cabos block (Walawender et al., 1990; Kimbrough et al., 2001; Kimbrough et al., 2002) and to the Half Dome Granodiorite of the central Sierra Nevada (Bateman, 1992).

The San Ignacio granodiorite (TKis) is named for exposures along the Rio Piaxtla at San Ignacio in the north-central part of the map area (HS-42; Fig. 2, Plate 1). The San Ignacio granodiorite is fine- to medium-grained equigranular and contains 7–15% anhedral biotite, hornblende, and clinopyroxene. Similar rocks crop out throughout the map area but cannot definitely be correlated. The modes of both San Ignacio and Candelero rock types vary considerably and overlap (Fig. 5).

Numerous other granitic rocks of small size or less distinctive character could not be assigned to either of these major posttectonic types. Four were correlated locally. Mafic quartz diorite (Colegio quartz diorite; Tic) petrographically and compositionally similar to some of the syntectonic types but lacking foliation crops out ~50 km north of Mazatlan. Fine-grained granodiorite and quartz monzonite (Concordia granodiorite; TKin) containing 1 cm poikilitic orthoclase underlie a 100 km^2 area ~30 km east-northeast of Mazatlan. Coarse-grained, K-feldspar-poor granodiorite (El Carmen granodiorite; TKie) underlies an area of ~100 km^2 south of the San Ignacio pluton. A small (15 km^2), fine-grained diorite pluton (Copala diorite; TKid) crops out around Copala along the Mazatlan-Durango highway, is commonly hydrothermally altered, and hosts some of the silver ore there.

Posttectonic intrusions are well dated by both U-Pb and K-Ar (Tables 1 and 2). The range of ages are again anchored by U-Pb dates of 67 Ma (HS-42; San Ignacio granodiorite), 48 Ma (HP-28; Candelero granodiorite), and 20 Ma (HS-53; Colegio quartz diorite). Most intrusions are concordant, which we interpret to date the time of emplacement. The oldest posttectonic rocks are sample HP-6 (biotite, 81.8 ± 0.9 Ma; hornblende, 82.6 ± 1.8 Ma) in the main map area and sample HC-5 (biotite, 88.6 ± 1.0 Ma; hornblende, 89.5 ± 2.0 Ma) from the northern transect. The next youngest intrusion is El Carmen granodiorite, with samples HS-12, HS-13, and HS-25 indicating an emplacement age ca. 75 Ma. Ages on other samples range nearly continuously to 46 Ma with a clear geographic pattern. Oldest ages are near the coast, and youngest ages are farthest inland.

In addition to the U-Pb and K-Ar dates on sample HS-42, concordant dates or hornblende dates on the type pluton of the San Ignacio granodiorite are all ca. 64 Ma (HP-2, HS-40, HS-41, HP-11; Table 1). Samples 170 and 156 to the east are also ca. 64 Ma and may be from a continuation of the main pluton. San Ignacio granodiorite intrusions farther east have more equivocal ages. Biotite from sample 146 was reset to the 47 Ma age of the adjoining Candelero granodiorite, and hornblende was at least partly reset to 50 Ma. Sample HP-26 has only a biotite date of

49 Ma, which may indicate resetting also. Emplacement ages of these eastern intrusions are not established.

The K-Ar and U-Pb data indicate that the Candelero granodiorite was emplaced at several different times. The pluton of the type locality is ca. 48 Ma (HP-28, HP-14, HP-25). The westernmost example is concordant at ca. 82 Ma (HP-6), two different plutons in the north-central part of the map area are concordant at 62 Ma (HP-13) and 52 Ma (236), and the easternmost example has only a biotite date of 44 Ma (HP-18). A Candelero pluton along the northern transect is concordant at ca. 51 Ma. As is recognized in other Cordilleran batholiths, petrographically similar intrusions can be emplaced at different times.

Several biotite ages on major intrusions are still younger at 29 Ma (227), 31 Ma (HP-20), and 34 Ma (HP-23). The latter two samples are part of a Candelero-type intrusion in the northeasternmost part of the map area. The true age of this intrusion is at least 44 Ma, the biotite age of HP-18, and the young ages probably indicate reheating. Later magmatism in that area is indicated by a biotite age of 32 Ma on a large diorite dike (HP-24). The young biotite age of sample 227 in the north-central part of the map area may also indicate reheating rather than time of emplacement. Later magmatism in that area is indicated by a hornblende age of 30 Ma on an andesite dike (HP-10).

Similar posttectonic intrusions are recognized along the northern Sinaloa transect. In addition to the 89 Ma intrusion (HC-5) and the Candelero type intrusion with a concordant age of ca. 51 Ma, sample HC-6 gives a concordant age of ca. 67 Ma. The northeasternmost sample along that transect has only a 53-Ma biotite date (KC-3).

Chemical Characteristics and Spatial Variation

Granitic rocks of the Sinaloa batholith show compositional variations similar to those of other Cordilleran batholiths (Table 3, Figs. 4 and 6). Sinaloa granitic rocks are calcalkaline but border on calcic. Including two gabbros, SiO_2 contents of analyzed rocks range from 47 to 74%; excluding gabbro, the lower limit is 54%. Most major oxides vary smoothly with SiO_2, with incompatible elements such as TiO_2 and CaO decreasing and K_2O increasing with SiO_2. Trace elements show considerably more scatter, but Rb, Ba, La, Th, and U clearly increase with increasing SiO_2; V, Sr, and Sc decrease. Some, including Y and Nb, show no apparent correlation with SiO_2.

Both gabbros contain less than 50% SiO_2 and have very low K_2O and Rb concentrations (Table 3). Although sample HS-48 contains modal quartz, it is chemically equivalent to the gabbros, not the quartz gabbros, of the Peninsular Ranges batholith (Silver and Chappell, 1988). Rare earth element patterns are relatively flat (Fig. 7). Sample HS-46 shows a positive Eu anomaly that suggests it is a plagioclase cumulate, which is consistent with its high CaO and Al_2O_3 concentrations. Gabbros commonly plot off trends of the other granitic rocks, which is most noticeable for TiO_2 and Nb. Compared to the gabbros of the Peninsular Ranges, the Sinaloa gabbros have similar patterns but much higher total rare earth elements (REE) (Gromet and Silver, 1987) and higher concentrations of many incompatible trace elements (Walawender and Smith, 1980).

Syntectonic intrusions are dominated by mafic compositions. SiO_2 contents of seven out of nine analyzed syntectonic rocks range narrowly between 59 and 62% with one each at 65 and 67%. They are moderately enriched in light rare earth elements (LREE) and have small negative Eu anomalies (Fig. 7). Sample HS-44 is unusual in having very low total REE and a small positive Eu anomaly.

Posttectonic rocks have a wider compositional range, from 54 to 74% SiO_2, than do syntectonic rocks (Table 3, Figs. 4 and 6). However, with a few exceptions, rocks containing less than ~63% SiO_2 are minor border phases (HS-40, HS-41) or small intrusions (HP-7, 199). Other major oxides and trace elements reflect these differences. Posttectonic rocks have lower TiO_2, Al_2O_3, CaO, total Fe, MnO, MgO, P_2O_5, and Sr and higher K_2O, Rb, Th, and U than do syntectonic rocks. Some trace elements show little difference, including Zr, Nb, and, despite general correlation with SiO_2, Ba and most REE.

The Candelero and San Ignacio granodiorites are compositionally as well as petrographically distinct. SiO_2 concentrations in Candelero samples range from ~64 to 72% and in San Ignacio samples from 62 to 67% (excluding sample HS-41, which is a plagioclase concentrate). They also have distinct REE patterns with similar LREE abundances, but Candelero samples have lower heavy rare earth element (HREE) (and Y) abundances and smaller Eu anomalies (Fig. 7).

Samples HS-40 and HS-41 are border phases of the San Ignacio pluton. The composition of HS-41, including high Al_2O_3, CaO, and Sr, indicates it is a plagioclase concentrate, which is consistent with outcrop and thin section characteristics. Sample HS-40 also has high Sr, but other major oxides are not unusual. Both samples have unusual REE patterns with low total REE and prominent positive Eu anomalies consistent with plagioclase accumulation.

The granitic rocks show distinct spatial chemical patterns (Fig. 8). With much scatter, SiO_2 increases eastward, which reflects the distribution of more mafic syntectonic and more silicic posttectonic rocks. Many major oxides and trace elements show similar patterns reflecting their variation with SiO_2 but also with considerable scatter. The Colegio tonalite is a notable exception of a relatively mafic posttectonic intrusion. It is compositionally like the syntectonic rocks and crops out near the coast with them. This indicates that the compositional variation is a function of location, not of age.

To look for spatial patterns that are not simply related to variations in SiO_2, we used a subset of the granitic rocks containing between 63 and 67% SiO_2 (Fig. 9). For this subset, SiO_2 shows at most a slightly negative correlation with location. Nevertheless, TiO_2, Rb, Zr, Pb, Th, U, and REEs show considerable scatter but increase eastward; Ba and Sr decrease. Other elements show no discernible pattern. Location apparently plays a role in magma composition, and a variety of factors are possible, but further interpretation is beyond the scope of this report.

Sr isotope compositions determined on six samples range from 0.7030 to 0.7062 (Table 3) (Note: analysis of sample HP-28

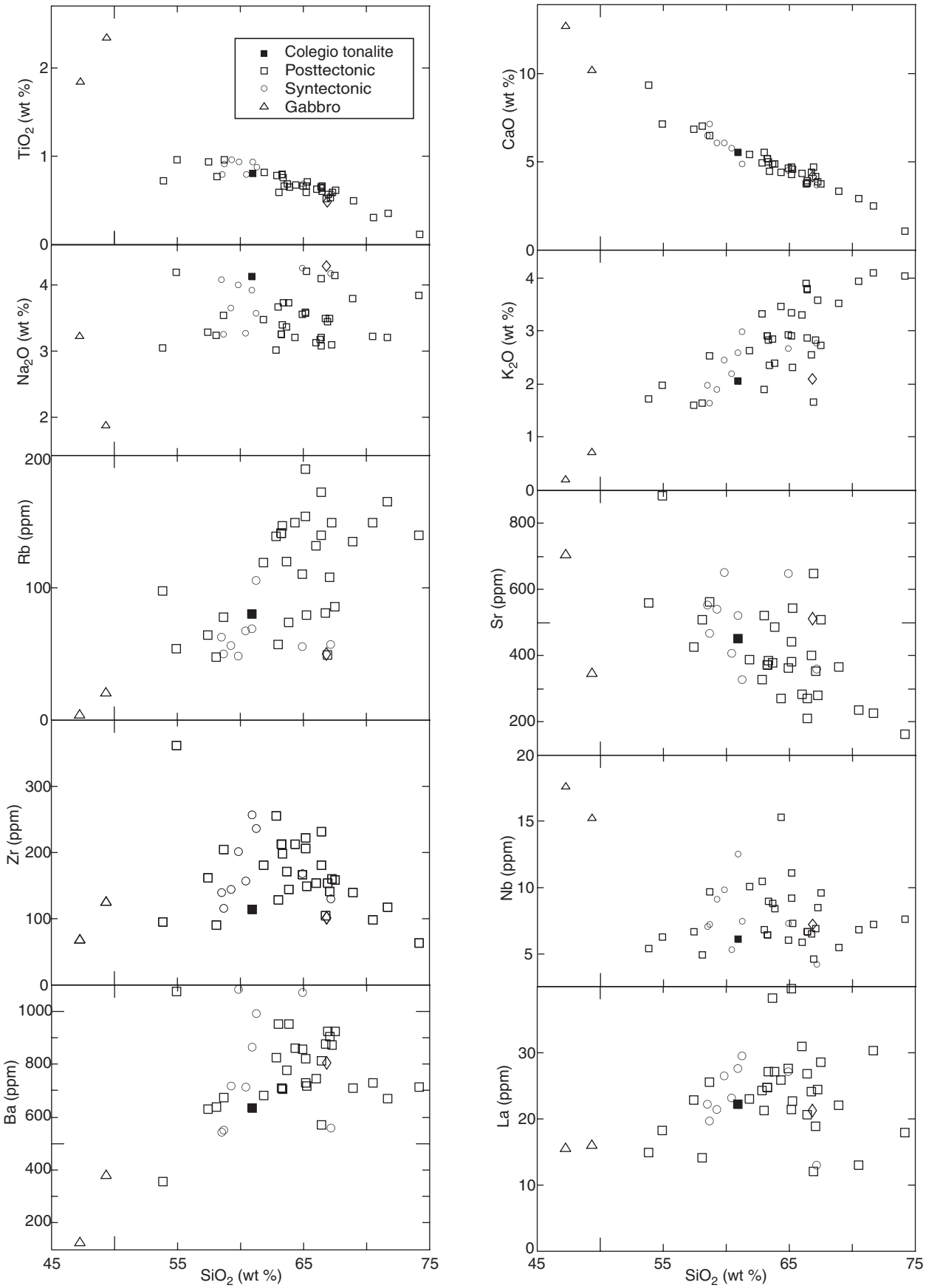

Figure 6. Harker variation diagrams for selected major oxides and trace elements.

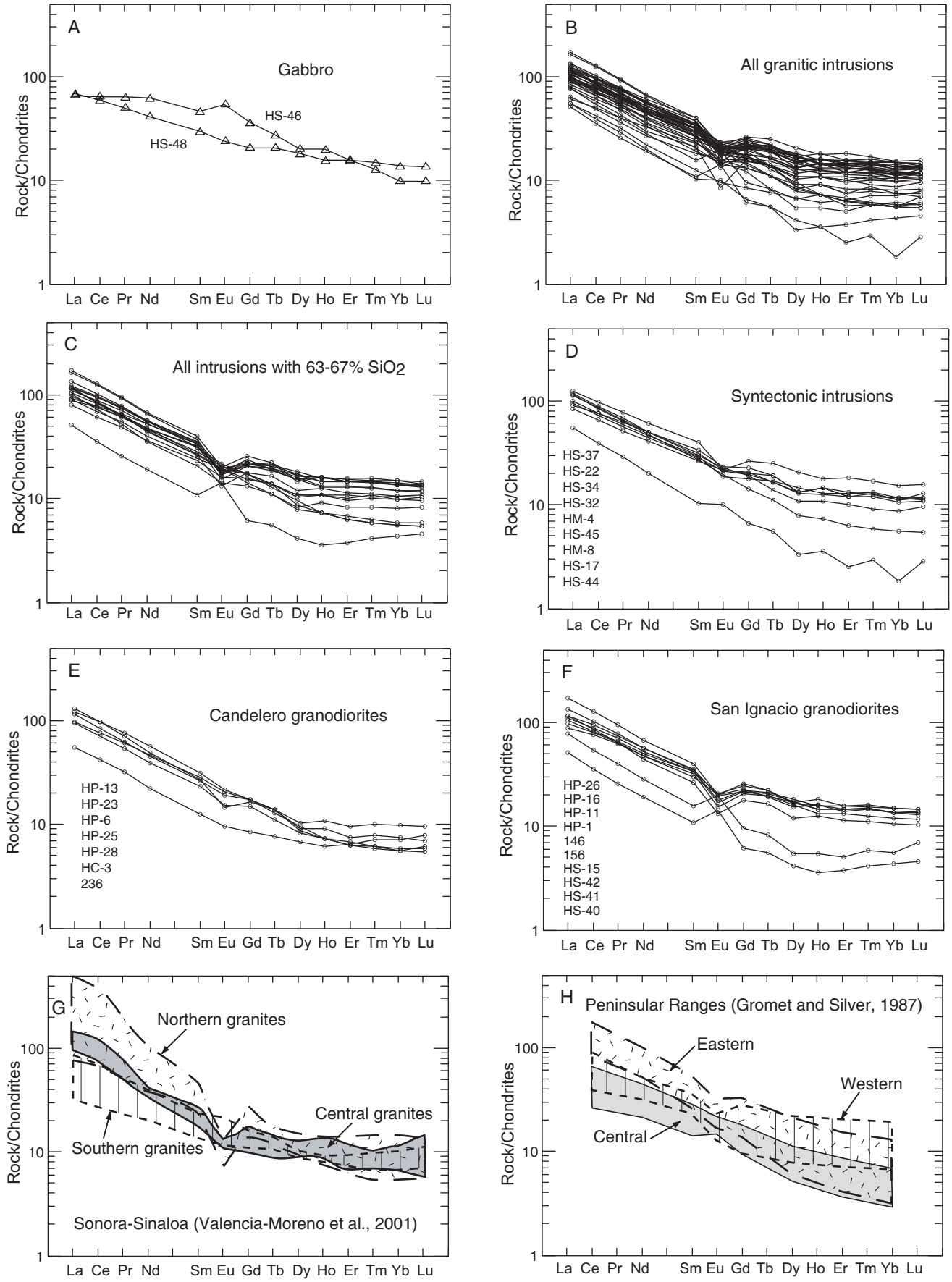

Figure 7. Chondrite normalized rare earth element patterns for rocks of Sinaloa batholith (normalization values from Anders and Grevesse, 1989). A: Gabbros. B: All granitic rocks of batholith. C: All granitic rocks containing between 63 and 67% SiO_2. D: Syntectonic intrusions. E: Candelero granodiorites. F: San Ignacio granodiorites. In D, E, and F, sample numbers are listed in decreasing order of La abundance. G: REE patterns of batholithic rocks of Sonora and Sinaloa from Valencia-Moreno et al. (2001). H: REE patterns of rocks of Peninsular Ranges batholith from Gromet and Silver (1987).

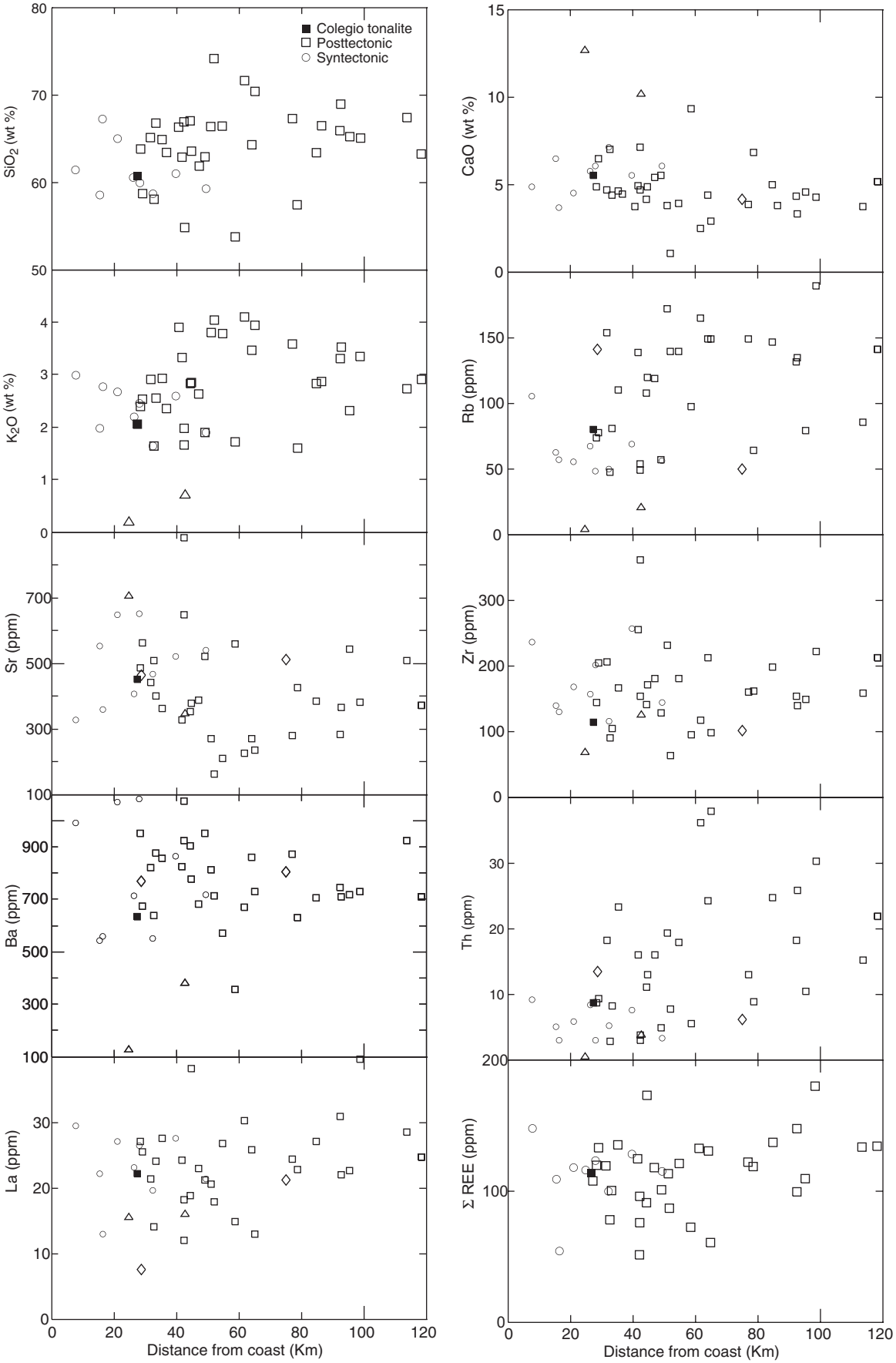

Figure 8. Plots of composition versus distance from an arbitrary, north-northwest line along Pacific coast. SiO_2 content generally increases eastward but with considerable scatter. Much of gradient reflects lack of more mafic plutons to east, such as syntectonic intrusions. Similarly, major oxides (CaO and K_2O) and trace elements that vary with SiO_2 (Rb, Sr, Zr, Ba, and Th) also show compositional gradients but also with considerable scatter. The 20 Ma Colegio tonalite is compositionally like syntectonic rocks and crops out near coast with them. This indicates that compositional variation is a function of location, not age.

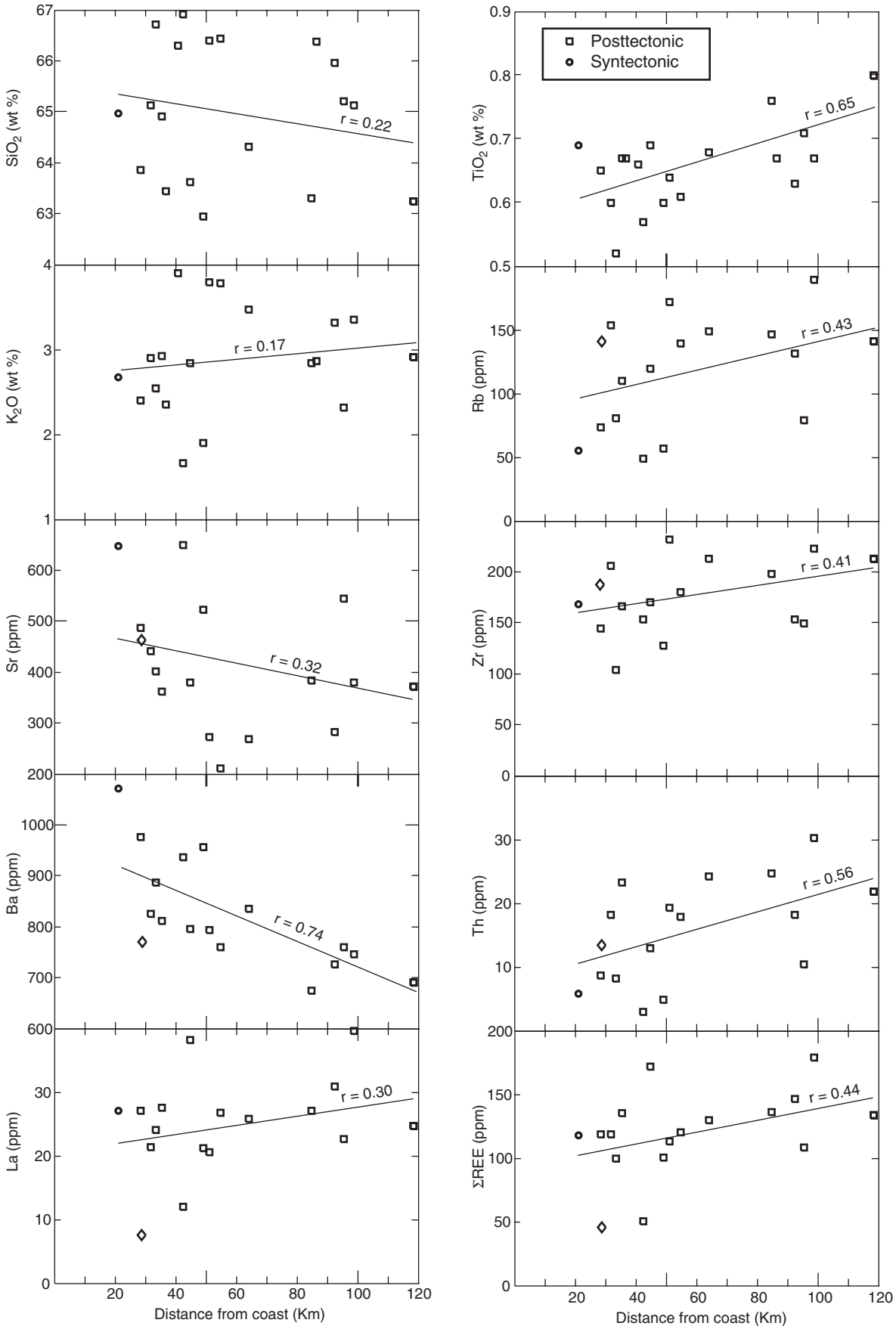

Figure 9. Variation in composition with location for samples containing between 63 and 67% SiO_2. Location is based on same arbitrary, north-northwest line used in Figure 8. SiO_2 exhibits at most slightly negative correlation with location. With considerable scatter, some major oxides and trace elements increase with distance from coast, including TiO_2, Rb, Zr, Th, U, La, and total REE. Ba and Sr decrease with distance. (Regression lines and correlation coefficients using IgPet99 developed by Michael Carr).

in 1973 gave an initial ratio of 0.7163. Reanalysis in 2002 gave 0.7044. We interpret the reanalysis to be correct and the old analysis to have been contaminated. An initial ratio of 0.7044 is consistent with the other five samples and the following published data). Damon et al. (1983a) report initial ratios on granitic rocks of 0.7042 from La Azulita, which lies ~6 km northeast of sample HS-23, and of 0.7052 from Cosala, which lies ~40 km north of sample HP-5 (Fig. 2, Plate 1). Valencia-Moreno et al. (2001) report an initial ratio of 0.70256 on their sample Mal-74, which is from the same location as sample KC-1. All ratios fall within the range of southern granites of Valencia-Moreno et al., which lie within the Guerrero terrane underlain by Mesozoic volcanic and sedimentary rocks and apparently lacking a Precambrian basement.

Lower Volcanic Complex (TKv)

The informally named lower volcanic complex (McDowell and Keizer, 1977) crops out chiefly in the eastern parts of the map area (upper Rio Piaxtla and Rio Presidio valleys of Plate 1), where it is generally coextensive with the posttectonic plutons. The lower volcanic complex is composed of andesitic to rhyolitic lavas, rhyolitic ash-flow and air-fall tuffs, volcaniclastic sedimentary rocks, and minor hypabyssal intrusions. They are almost everywhere propylitically altered and are the hosts of many of the major ore deposits of the area and the Sierra Madre Occidental (Wisser, 1965; Smith et al., 1982; Clarke and Titley, 1988).

The best-studied sections are around the major silver-gold mines of Tayoltita in the northeastern part of the map area and Panuco in the southeastern part (locations GD and HS-51 of Fig. 2, Plate 1). At Tayoltita, ~1200 m of rhyolitic tuffs and possible lavas are overlain by ~800 m of andesite lavas (Nemeth, 1976). Rhyolites contain phenocrysts of quartz, sanidine, biotite, and plagioclase. Feldspars are commonly altered to sericite and biotite to chlorite. One of the tuffs contains clasts up to 1 m in diameter, indicating a local source. Andesites and possibly equivalent hypabyssal intrusions contain plagioclase and clinopyroxene phenocrysts in fine-grained groundmasses of plagioclase laths, clinopyroxene, and opaque minerals. At Panuco, rhyolitic tuffs and lava flows predominate over andesitic lavas (T. Albinson and R.L. Leisure, personal commun., 1982).

Field relations and a few K-Ar ages suggest that lower volcanic rocks are broadly contemporaneous with the posttectonic rocks and are, in part, their extrusive equivalents. The lower volcanic rocks are generally coextensive with the posttectonic rocks. Lower volcanic rocks directly overlie metasedimentary rocks near Panuco (HS-51) and north of San Ignacio (HS-42) and have not undergone regional metamorphism or folding. Most contacts between lower volcanic rocks and granitic rocks are intrusive. However, lower volcanic rocks accumulated upon the eroded surface of a granodiorite pluton (HS-51 with a minimum age of 51 Ma) near Panuco, and Albinson (personal commun., 1982) found granitic boulders in agglomerates within the lower volcanic complex near Panuco. Granitic inclusions occur in tuffs of the lower volcanic complex in the northern part of the map area. Rhyolitic dikes, petrographically similar to rocks of the lower volcanic complex, cut granitic rocks in several areas near San Ignacio.

Because of their alteration, lower volcanic rocks have not been directly dated anywhere in the map area. On the northeast side of the Sierra Madre Occidental, an andesitic lava 40 km southeast of Durango City is dated at 53 Ma (McDowell and Keizer, 1977), and a sequence of rhyolitic tuffs and andesitic lavas near Nazas 130 km north of Durango are 51–40 Ma (Aguirre-Díaz and McDowell, 1991). Recent U-Pb dating of equivalent rocks in eastern Sonora has shown that they are as much as 20 Ma older than the plutons of the local batholith (McDowell et al., 2001). Hence, the Lower Volcanic Complex may be an important but undated part of the magmatic record in southern Sinaloa.

Oligocene-Miocene Magmatism

Both U-Pb and K-Ar ages confirm the young, 20 Ma age of the Colegio quartz diorite. Although 25 Ma younger than any other dated large intrusion, it is, nevertheless, a large, coarse-grained intrusion indistinguishable from other posttectonic intrusions without the isotopic ages. It demonstrates major batholithic activity at 20 Ma.

Although the Colegio quartz diorite is the only identified large young pluton, several other minor intrusions, as well as lavas and tuffs, are also Oligocene or Miocene (Henry and Fredrikson, 1987; Aranda-Gómez et al., 1997). In addition to the dikes mentioned above, these include a dacite lava in the southernmost part of the map area (22 Ma; HM-1), a rhyolite dike in the northern part (24 Ma; 174), an ash-flow tuff in the north-central part (28 Ma; 3–7-10), and another tuff in the central part (17 Ma; F-8–1). Except for the two tuffs, for which source calderas are not known, these indicate local magmatism at those times.

These young ages indicate that magmatism in Sinaloa was coeval with the upper volcanic sequence of the Sierra Madre Occidental and the Miocene volcanic arc of Baja California. All known sources of ash-flow tuffs of the upper volcanic sequence are in Durango to the east (McDowell and Keizer, 1977; Swanson et al., 1978; McDowell and Clabaugh, 1979; Swanson and McDowell, 1984; Nieto-Samaniego et al., 1999). However, our reconnaissance mapping in Sinaloa could have missed major sources. Furthermore, many other small intrusions, lavas, and ash-flow tuffs are undated but undoubtedly late Tertiary (e.g., Tif of Plate 1). The Miocene volcanic arc, so well known around the rest of the Gulf of California (Gastil et al., 1979; Hausback, 1984; Sawlan, 1991; Mora-Alvarez and McDowell, 2000), may be well represented in Sinaloa. Basaltic volcanism at 11 and 2–3 Ma records the change to extension around the Gulf of California (Aranda-Gómez et al., 1997; Henry and Aranda-Gómez, 2000).

DISCUSSION

Overall Timing and Continuity of Magmatism

The combined U-Pb and K-Ar ages document magmatism in southern Sinaloa from at least 101 to 20 Ma. Gabbro intru-

sion may have begun as early as 138 Ma, but interpretation of the two gabbro hornblende ages is uncertain. Intrusion of mafic tonalites began at least by 101 Ma. Many of the tonalites show dynamic crystallization textures that indicate they were emplaced before or during a major deformational episode. Based upon the estimated maximum of 450 °C, this deformation would likely have reset biotite K-Ar ages but probably not hornblende K-Ar ages. Uncertainty in the interpretation of the K-Ar ages of these early mafic rocks allows either that they were emplaced between ca. 101 and 90 Ma, or that many if not all of the syntectonic intrusions were emplaced before 101 Ma. Some must be younger than ca. 110 Ma, the probable age of Aptian limestone that they intrude. Posttectonic intrusions began to be emplaced as early as 82 Ma in southern Sinaloa and 89 Ma in northern Sinaloa. No intrusions are dated between 89 and 82 Ma, between 82 and 75 Ma, or between 62 and 56 Ma, but batholith emplacement was apparently prolific between 75 and 45 Ma (Fig. 3). Another gap for granitic bodies falls between 45 and 20 Ma, although several minor intrusions fall within that time.

Whether these gaps indicate a real hiatus in magmatism or simply incomplete exposure or sampling and to what extent the volumes of magmatism have varied through time are uncertain. The mapped area is large but still small relative to the distribution of batholiths along the west coast of México (Fig. 1). Based on the distribution of ages, intrusions between 89 and 82 and 82 and 75 Ma should reside near the Pacific coast (Figs. 2 and 10A, Plate 1). Much of that area is covered by younger rocks, especially along our Rio Piaxtla transect. Additional sampling of granitic rocks in areas where access has improved since 1972 would be useful. Except for the possible age gaps, outcrop areas and therefore probable volumes of granitic rocks seem similar between 100 and 45 Ma. Certainly, no time dominates the record of batholithic emplacement in southern Sinaloa.

The age pattern suggests that intrusions younger than 45 Ma might be present beneath tuffs of the upper volcanic sequence, which form a nearly complete cover in the Sierra Madre Occidental. The ash-flow tuffs of the Sierra Madre erupted from numerous calderas (Swanson and McDowell, 1984) that are almost certainly underlain by major plutons (Lipman, 1984). Aguirre-Díaz and McDowell (1991), who found the 51–40 Ma rhyolites and andesites near Nazas (Fig. 1), identified many other areas of Eocene magmatism around the Sierra Madre and suggested that an Eocene volcanic field was as extensive as the mostly Oligocene Sierra Madre (McDowell and Clabaugh, 1979).

Eastward Shift of Magmatism

The Sinaloa batholith shows a distinct geographic age pattern (Fig. 10, A and B). Oldest ages are near the coast and youngest ages are farthest east. Whether the syntectonic rocks are part of an eastward trend is uncertain. The first uncertainty is whether the K-Ar ages of the syntectonic rocks indicate emplacement times. Even if they do, the ages do not correlate with location (Fig. 10A). Both the age uncertainty and the narrow, 50-km width of their distribution limit interpretations about migration.

The age pattern for the posttectonic rocks is more obvious. Ages decrease progressively eastward from between 80 and 90 Ma, within 20–30 km of the Pacific Ocean, to ca. 45 Ma, 120 km from the coast at the western edge of the Sierra Madre Occidental. The six samples from our reconnaissance transect in northern Sinaloa show the same pattern. Critical information that is missing is timing for the volcanic rocks of the Lower Volcanic Complex. Though they are generally presumed to be coeval with the batholiths, they have not been dated in Sinaloa and most other areas due to their general alteration. One andesitic lava, possibly equivalent to the Lower Volcanic Complex in Durango has a K-Ar age of 53 Ma (McDowell and Keizer, 1977).

Another uncertainty is whether rocks of the upper volcanic sequence of the Sierra Madre Occidental represent a continuation of the same eastward shift of magmatism. Near Durango City, these rocks are 32–28 Ma (McDowell and Keizer, 1977; Swanson et al., 1978; Aranda-Gómez et al., 1997), which is consistent with a continued eastward migration of magmatism.

Upper Cretaceous and Eocene igneous rocks near Nazas (Fig. 1) constitute the only known exceptions to the regional age pattern. A small (<1 km^2) diorite intrusion is dated at 88 Ma (hornblende K-Ar), two ash-flow tuffs (with unknown sources) are 51 and 43 Ma, and andesite lavas are 49 and 45 Ma (Aguirre-Díaz and McDowell, 1991). The pluton and andesites are as old as or older than the youngest plutons dated in southern Sinaloa and demonstrate that older igneous activity did occur locally along the eastern margin of the Sierra Madre Occidental.

The age data also indicate a westward return, but that is based on many fewer ages and with significant data gaps and uncertainties in source locations (Fig. 10B). Within the Sierra Madre, the youngest (23 Ma) volcanic rocks are in its western part, just east of the area of Figure 2 (McDowell and Keizer, 1977). Ages for the 20 Ma Colegio quartz diorite (HS-53) and the 22 Ma rhyodacite lava (HM-1) may reflect a continuation of this westward trend.

Rates of migration can be calculated from the age patterns (Fig. 10), but distances need to be corrected for Miocene and later extension (Henry, 1989; Henry and Aranda-Gómez, 2000). Extension affected only the region west and east of the relatively unextended block of the Sierra Madre Occidental. Fortunately, extension paralleled the direction of igneous migration. Using only the ages of posttectonic rocks and correcting for as much as 50% east-northeast extension, the eastward sweep progressed at a rate of ~1.5 km/Ma. If syntectonic rocks or at least the 101-Ma Recodo tonalite are included, the rate decreases to as little as 1 km/Ma. The apparent westward shift was much more rapid at ~12–15 km/Ma.

Comparison with Batholiths of Western México

The Sinaloa batholith shares marked similarities and some differences with the Peninsular Ranges batholith of southern and Baja

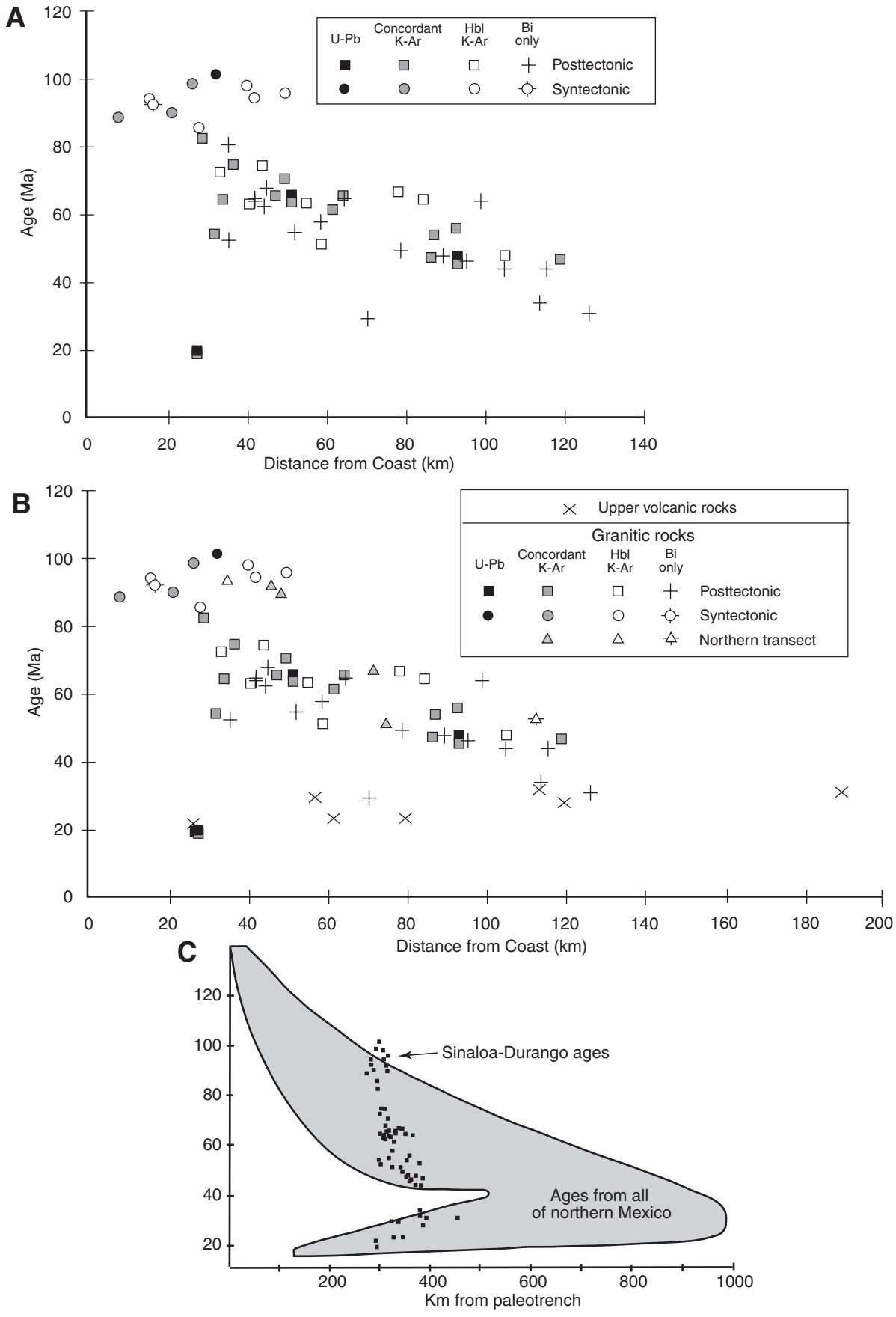
A
U-Pb
Concordant K-Ar
Hbl K-Ar
Bi only
Posttectonic
Syntectonic
Age (Ma)
Distance from Coast (km)
B
Upper volcanic rocks
Granitic rocks
U-Pb
Concordant K-Ar
Hbl K-Ar
Bi only
Posttectonic
Syntectonic
Northern transect
Age (Ma)
Distance from Coast (km)
C
Sinaloa-Durango ages
Ages from all of northern Mexico
Km from paleotrench

Figure 10. Plots of age of igneous rocks versus distance from same north-northwest line as Figure 8. A: Only granitic rocks from main map area (Fig. 2). Posttectonic rocks show eastward migration of intrusion between ca. 82 and 45 Ma. Allowing for ~50% east-northeast extension across area, calculated rate of eastward migration is ~1.5 km/Ma. The 45 Ma rocks crop out in deep canyons of Sierra Madre Occidental; any granitic rocks, if present farther east, are covered by tuffs of Sierra Madre. Although oldest, syntectonic rocks are closest to coast, individual syntectonic rocks show no apparent relation between K-Ar age and location. B: Age plot with addition of granitic rocks from northern Sinaloa transect and upper volcanic rocks from southern Sinaloa and Durango (Durango data from McDowell and Keizer, 1977). Granitic rocks of northern transect show same pattern as do rocks of southern Sinaloa. Ages and distribution of upper volcanic rocks suggest westward return of magmatism at ~12–15 km/Ma. C: Age plot of Figure 10A placed on plot of Damon et al. (1981), who compiled ages including data of this study from a 1200-km-long, arc-parallel swath from México-U.S. border to Trans-Mexican volcanic belt onto single east-northeast transect. Magmatism migrated much farther inland in northern México and southwestern United States (Coney and Reynolds, 1977) than it did in southern Sinaloa.

California, batholithic rocks of Sonora, the batholith of the Cabo San Lucas block at the tip of Baja California, and batholithic rocks that crop out from Jalisco eastward to Oaxaca in southern México (Fig. 1, Table 4). The strongest similarities are in the types of intrusions, sequence from early gabbro through commonly mafic pre- or syntectonic intrusions to more felsic posttectonic intrusions, and general eastward migration of magmatism. The major differences are in the range of ages, probable depth of emplacement and concordant versus discordant ages, and the short distance and much slower rate of eastward migration in Sinaloa compared to that for either the Peninsular Ranges or Jalisco-Oaxaca. Sinaloa rocks share both compositional similarities and differences with rocks of the Peninsular Ranges and Sonora.

Early, layered gabbros that range from peridotite to anorthosite and hornblende gabbro and which formed through cumulate processes are prominent in all four areas (Gastil, 1975; Gastil et al., 1979; Todd and Shaw, 1979; Walawender and Smith, 1980; Hausback, 1984; Aranda-Gómez and Perez-Venzor, 1989; Schaaf et al., 1997). Hornblende K-Ar ages of gabbros in the Peninsular Ranges range from 129 to 146 Ma (Krummenacher et al., 1975) but have been interpreted to indicate excess Ar (Silver et al., 1979). The only U-Pb date on gabbro in the Peninsular Ranges is 111 ± 1 Ma, and this dated gabbro is not the same as the gabbros that have K-Ar ages (Silver et al., 1979). A single hornblende K-Ar date of 115 Ma is reported in the Cabo San Lucas block (Hausback, 1984). Gabbro is abundant in western Jalisco near the Pacific Ocean, but the only dated rock is a gabbro pegmatite farther east in Nayarit (hornblende, 97.6 ± 2.6 Ma; Gastil et al., 1979; Schaaf et al., 1995). Gabbros of Sinaloa appear to be similar to those of the Peninsular Ranges batholith in major oxides but have substantially higher REE and incompatible trace element concentrations (Walawender and Smith, 1980; Gromet and Silver, 1987; Walawender et al., 1991). A significant difference is that gabbro in Sinaloa crops out with granitic rocks that were contemporaneous with the younger (105–80 Ma), eastern part of the Peninsular Ranges batholith, where gabbro is minor.

Pre- or syntectonic intrusions are concentrated in the western part of the Peninsular Ranges (Silver et al., 1979; Todd and Shaw, 1979; Todd et al., 1988). They are also present in the western part of the Cabo San Lucas block (Aranda-Gómez and Perez-Venzor, 1989), but their distribution is otherwise unknown. No data are available about the presence of syntectonic rocks in the Jalisco-Oaxaca transect. Syntectonic rocks are dominantly low-K tonalites to granodiorites rocks in Sinaloa, the Peninsular Ranges, and Cabo San Lucas but include more felsic rocks in the Peninsular Ranges and Cabo San Lucas (Silver et al., 1979; Todd and Shaw, 1979; Aranda-Gómez and Perez-Venzor, 1989).

All areas except Jalisco, for which no data are available, and probably Sonora underwent intense deformation, but the end of this deformation may be different in each area. Deformation ended ca. 105 Ma in the Peninsular Ranges, essentially coincident with the beginning of eastward migration of magmatism (Silver et al., 1979; Todd and Shaw, 1979; Todd et al., 1988; Johnson et al., 1999b). An intensely deformed zone that forms the boundary between older, deformed granitic rocks on the west and younger, undeformed rocks on the east may be a suture between an outlying island arc and North America (Todd et al., 1988; Johnson et al., 1999b). The end of deformation is not as well dated in Sinaloa or in the Cabo San Lucas block. Depending on interpretations of K-Ar dates on syntectonic rocks in Sinaloa, the change may have occurred before 101 Ma but definitely had occurred by 89 Ma. Whether the beginning of eastward migration of magmatism accompanied this change, as it did in the Peninsular Ranges, is unclear because the eastward migration was so slow. The change probably occurred ca. 98 Ma in the Cabo San Lucas block (Frizzell et al., 1984; Aranda-Gómez and Perez-Venzor, 1989).

Posttectonic intrusions were emplaced in all areas and were accompanied by an eastward migration, although whether an eastward migration also occurred in the Cabo San Lucas block is unknown. Post- and syntectonic intrusions overlap spatially more in Sinaloa than in the Peninsular Ranges, where posttectonic rocks are almost exclusively east of the belt of syntectonic intrusions. Posttectonic intrusions are heavily dominated by more potassic and felsic compositions, mostly >62% SiO_2 in Sinaloa, the Peninsular Ranges (Silver et al., 1979; Silver and Chappell, 1988; Baird and Miesch, 1984), and Sonora (Roldan-Quintana, 1991; McDowell et al., 2001; Valencia-Moreno et al., 2001; Housh and McDowell, unpublished data) and high-K granodiorite and granite in the Cabo San Lucas block (Aranda-Gómez and Perez-Venzor, 1989; Kimbrough et al., 2002). A difference is that tonalite dominates in the Peninsular Ranges whereas granodiorite dominates in Sinaloa and Sonora. Also, the Peninsular Ranges are calcic whereas the Sinaloa batholith is borderline calc-alkalic (Fig. 4; Table 4). Granodiorite and monzongranite dominate in the Cabo San Lucas block (Frizzell, 1984; Aranda-Gómez and Perez-Venzor, 1989; Schaaf et al., 1997; Kimbrough et al., 2002).

TABLE 4. BATHOLITH COMPLEXES OF WESTERN MEXICO

Batholith complex	Sinaloa	Peninsular Ranges—Sonora		Cabo San Lucas	Jalisco—SW Mexico
		Peninsular Ranges	Sonora		
General composition	Borderline calc-alkalic/calcic	Calcic	Calc-alkalic		Calc-alkalic
Dominant rock type or range	Granodiorite	Tonalite	Granodiorite to quartz monzonite	Tonalite to monzogranite	Tonalite to granite
Rock type progression	Early gabbro, syntectonic mafic quartz diorite and tonalite, posttectonic granodiorite and monzogranite	Early gabbro, syntectonic tonalite to granodiorite, posttectonic leucocratic tonalite and granodiorite	Unknown	Early gabbro, syntectonic tonalite and trondhjemite, posttectonic leucocratic granodiorite and monzongranite	?
Granitic duration	101–45 Ma, 20 Ma	140-80 Ma	90–50 Ma	ca.100–70 Ma	ca.103–25 Ma
Gabbro type	Layered gabbro, pyroxenite, anorthosite	Layered hornblende gabbro, norite, and peridotite	Gabbro not present	Layered hornblende gabbro, pyroxenite, anorthosite	Gabbro present but not described
K-Ar ages	134, 139 Ma	129, 133, 146 Ma		115 Ma; 129 ± 15 Ma (Rb/Sr)	98 Ma
Distribution	Mostly in west	Very dominantly in west		Dominantly in west?	Abundant in west near Puerto Vallarta, but also reported farther east at Zihuatanejo
Syntectonic rocks	Mafic quartz diorite and granodiorite	Mafic quartz diorite and granodiorite accompanied by leucocratic granodiorite	Not present?	Tonalite and trondhjemite	Not definitely present
Posttectonic rocks	Granodiorite and granite	Tonalite to low-K granodiorite		Tonalite to granite	Quartz diorite to granite
S-type (Two-mica granites) present?	No	Yes, mostly on east side	Minor two-mica granite	Yes	Yes in Jalisco (Puerto Vallarta batholith) at west end
Syn/post overlap?	Yes, a lot	Very little?	?	Yes	?
Syn/Post change	>90 Ma	105 Ma	?	98 Ma	?
Eastward migration	Yes after 90 Ma, before?	Yes after 105 Ma	Yes	Probably	Yes
Distance	Batholiths: 120 km; adding Oligocene volcanic: 200 km	~100 km width of Peninsular Ranges	Plutons: 250 km @28°N - minus extension; total for northern Mexico ~1000 km		~600 km perpendicular to paleotrench
Rate	1–1.5 km/Ma	10 km/Ma	~6 km/Ma	?	~10 km/Ma
Westward return?	Yes, at ~12–15 km/Ma		Yes, rate very high (>50 km/Ma)	Yes, Miocene volcanic rocks abundant north of La Paz	No
Basement	Jurassic? metasedimentary	West: Mesozoic metasedimentary; east: Paleozoic and Mesozoic metasedimentary	North=Precambrian; central and south=Paleozoic eugeoclinal	Jurassic? metasedimentary, but granitic Sr and Nd data indicate Precambrian	Highly variable. West=Jurassic metasedimentary, but granitic Sr and Nd data indicate Precambrian; east=Precambrian
U-Pb/K-Ar age difference	Posttectonic=no; syntectonic=?	West: no; east: yes	West: unknown; east: probably		West: probably; east: no
Age gaps	89–82, 82–75, 62–56 Ma	No	No	?	No?
Sr initial	9 samples: .7026 to .7062	.703 on west to .708 on east	.706–.709; one value .713	average: .706; gabbros: .7035–.7039; granitic: .7048–.707; two-mica granites: .712–.716	Jalisco: .7038–.712; Oaxaca: .7037–.7054

Note: Data from this study and Anderson and Silver, 1974; Aranda-Gómez and Perez-Venzor, 1989; Damon et al., 1981, 1983; Ferrari et al., 2000; Frizzell, 1984; Frizzell et al., 1984; Gastil, 1975; Gastil et al., 1975, 1978, 1979; Hausback, 1984; Housh and McDowell, 1999, unpublished; Kimbrough et al., 2001; Martiny et al., 2000; McDowell and Mauger, 1994; McDowell et al., 2001; Moran-Zenteno et al., 2000; Nieto-Samaniego et al., 1999; Ortega-Rivera et al., 1997, this volume; Roldan-Quintana, J., 1991; Schaaf et al., 1995, 1997, 2000; Sedlock et al., 1993; Silver et al., 1979; Silver and Chappell, 1988; Stein et al., 1994; Tardy et al., 1994; Todd and Shaw, 1979; Todd et al., 1988; Valencia-Moreno et al., 2001; Walawender et al., 1990, 1991; Zimmermann et al., 1988

Muscovite-bearing rocks with high $^{87}Sr/^{86}Sr$ are present as minor components everywhere except Sinaloa.

The concordance of K-Ar ages and U-Pb ages in southern Sinaloa is a significant difference from the Peninsular Ranges, where K-Ar ages are generally discordant and the absolute age difference compared to U-Pb zircon ages increases eastward (Gastil, 1975; Krummenacher et al., 1975; Silver et al., 1979; Silver and Chappell, 1988; Snee et al., 1994; Ortega-Rivera et al., 1997; Ortega-Rivera, this volume, Chapter 11). The age pattern in Sinaloa indicates shallow emplacement and rapid cooling, which is consistent with the geological evidence of shallow emplacement (coexistence of plutons with coeval(?) volcanic rocks and epithermal ore deposits). The regional discordance in the Peninsular Ranges reflects regional uplift that exposed deep levels of the eastern part of the batholith long after intrusion.

Similarities and differences between Sinaloa, the Peninsular Ranges, and Cabo San Lucas extend to individual intrusive types. The Candelero granodiorite, La Posta suite, and Las Cruces granite are prominent, petrographically similar posttectonic intrusive types in Sinaloa, the Peninsular Ranges, and Cabo San Lucas respectively (Walawender et al., 1990; Kimbrough et al., 2001, 2002). They overlap compositionally and share petrographic characteristics of euhedral biotite and hornblende plus large, euhedral, honey-colored sphene (Walawender et al., 1990). REE patterns are indistinguishable with similar steep slopes and negligible Eu anomalies (Gromet and Silver, 1987). Marked differences include the lack of muscovite-bearing cores in Candelero intrusions, which are common in La Posta intrusions. Also, La Posta intrusions were emplaced over a narrow age range of 99–94 Ma in both the Peninsular Ranges and Cabo San Lucas (Kimbrough et al., 2001; Kimbrough et al., 2002), whereas Candelero rocks are younger and emplaced between 82 and 48 Ma.

Sinaloa rocks show compositional similarities and differences with batholithic rocks of the Peninsular Ranges and Sonora. The wide compositional range is a notable characteristic of the Sinaloa batholith (Figs. 4 and 6). Sinaloa rocks span most of the SiO_2 range seen in the Peninsular Ranges but are distinctly more potassic (Silver and Chappell, 1988). Similarly, they span most of the range of K_2O-SiO_2 relations seen for a suite of granitic rocks that extends from northern Sonora into Sinaloa as far south as the area of this study (Valencia-Moreno et al., 2001).

Comparison of the REE characteristics of Sinaloa rocks to those of the Peninsular Ranges and Sonora is particularly interesting (Fig. 7). Gromet and Silver (1987) found that REE patterns varied systematically west to east across the Peninsular Ranges batholith with abrupt changes between the western, central, and eastern belts. Similarly, Valencia-Moreno et al. (2001) found systematic changes south to north from southern Sinaloa to northern Sonora. In both cases, the REE patterns paralleled other compositional and isotopic trends and correlated with the nature of the crust. In the Peninsular Ranges, crust changes from Mesozoic turbidites or volcanic equivalents of the batholith on the west to Mesozoic and Paleozoic metasedimentary rocks containing Precambrian detritus on the east (Silver and Chappell, 1988). The northwestern Mexican transect is inferred to pass from poorly known Mesozoic rocks in Sinaloa, as in this area, northward to Proterozoic crust covered by Paleozoic eugeoclinal rocks in southern Sonora, and to exposed Proterozoic crust in central and northern Sonora (Housh and McDowell, 1999; Valencia-Moreno et al., 2001).

REE characteristics of Sinaloa rocks are most like those of the eastern belt of the Peninsular Ranges and central granites of Sonora (Fig. 7). However, Sinaloa rocks span much of the range of the western and central belts of the Peninsular Ranges and of the southern and northern granites of northwestern México. Compared to the Peninsular Ranges, Sinaloa rocks do not show the low HREE abundances of rocks of the central belt or the very flat overall patterns of the western belt. Compared to the Sonora-Sinaloa rocks, the Sinaloa rocks overlap with all but the most LREE-enriched of the northern granites and the most LREE-depleted of the southern granites. This is despite the fact that Sinaloa lies within the defined southern group of Valencia-Moreno et al. (2001) and that one of their samples comes from this field area (Mal-74 is from the same location as KC-1; Fig. 2, Plate 1). Indeed, the REE pattern of Mal-74 is distinctly unlike any of our samples. If these REE patterns are in any way related to the nature of the crust, they suggest that southern Sinaloa is underlain by either Precambrian crust or crust that has a significant Precambrian detrital component. However, Sr initial ratios are low and similar to other ratios reported by Valencia-Moreno et al. (2001) for their southern granites. Our U-Pb data show little or no evidence of old zircons in the four dated samples. The low Sr ratios and lack of old zircons support the interpretation that old crust is not present in southern Sinaloa or in the area of southern granites. Little is known about the nature of crust beneath central México east of Sinaloa (Sedlock et al., 1993), but Nd model ages of lower crustal xenoliths suggest that most of the area is underlain by Phanerozoic, probably Paleozoic, crust and lacks Precambrian basement (Ruiz et al., 1988).

Batholithic magmatism continued far later in Sinaloa, to 45 Ma, than in the Peninsular Ranges (80 Ma; Silver et al., 1979; Silver and Chappell, 1988; Ortega-Rivera, this volume, Chapter 11) or the Cabo San Lucas block (70–80 Ma; Frizzell, 1984; Frizzell et al., 1984; Aranda-Gómez and Perez-Venzor, 1989; Kimbrough et al., 2002). However, these differences disappear when one considers likely eastern limits to the overall distribution of magmatism. Magmatism of Sinaloa continued to ca. 30 Ma if the upper volcanic sequence of the Sierra Madre Occidental of Durango is included (McDowell and Keizer, 1977; Swanson et al., 1978; Aranda-Gómez et al., 1997). Similarly, plutonism continued eastward of the Peninsular Ranges to ca. 60 Ma in eastern Sonora (Anderson and Silver, 1974; Damon et al., 1981; McDowell et al., 2001). Caldera-forming volcanism with underlying plutons continued to ca. 30 Ma throughout the Sierra Madre Occidental and as far eastward as Chihuahua and Trans–Pecos Texas, which is the easternmost magmatism at that latitude (Henry et al., 1991; McDowell and Mauger, 1994). Tertiary rhyolitic magmatism in the southern Sierra Madre Occidental, opposite the southern end

of the Cabo San Lucas block, and in Jalisco (Fig. 1), appears to roughly parallel that in Sinaloa and Durango (Nieto-Samaniego et al., 1999; Ferrari et al., 2000). Numerous rhyolite domes were emplaced ca. 30 Ma in the Mesa Central east of the Sierra Madre. Volcanism then shifted westward with a major pulse ca. 24 Ma in the Sierra Madre (Nieto-Samaniego et al., 1999). Magmatism appears to have migrated only eastward, to as young as ca. 25 Ma, farther south along the Jalisco–Oaxaca trend (Schaaf et al., 1995; Martiny et al., 2000; Moran-Zenteno et al., 2000). However, the western and eastern halves of this trend had markedly different Late Cenozoic histories. Eastward displacement of the Chortis block truncated the southern México continental margin of the eastern half and removed older parts of the magmatic arc (Schaaf et al., 1995; Moran-Zenteno et al., 2000). The presence of ca. 100–70 Ma intrusions in Jalisco indicate that the western half was not truncated (Gastil et al., 1978; Zimmermann et al., 1988; Schaaf et al., 1995).

Regardless of whether this inland activity is included, differences still remain in the distances that magmatism migrated eastward and the rates at which it did so. The Sierra Madre Occidental is ~400 km east of a projected paleotrench (Fig. 10C) and was 300–350 km before "proto-Gulf" extension (Stock and Hodges, 1989; Henry and Aranda-Gómez, 2000). Likewise, Trans–Pecos Texas is ~1000 km east of the paleotrench and originally was 700–900 km, allowing for various estimates of extension across the Gulf of California, Sonora, and Chihuahua (Stock and Hodges, 1989; Gans, 1987; Henry and Aranda-Gómez, 2000). Magmatism migrated ~600 km northeastward perpendicular to the inferred position of the late Mesozoic–early Cenozoic paleotrench in the Jalisco–Oaxaca trend, but truncation of the continental margin again complicates interpretation (Schaaf et al., 1995; Moran-Zenteno et al., 2000).

The difference in migration rates is also striking. Silver and Chappell (1988) estimated that magmatism migrated at ~10 km/Ma across the Peninsular Ranges. A similar rate can be calculated farther east for migration across the eastern segment in Sonora, Chihuahua, and Texas. We calculate a similar 10 km/Ma for the Jalisco–Oaxaca trend, which is different than the still higher rates calculated in part along strike of the subduction zone by Schaaf et al. (1995). These rates are far more rapid than the 1–1.5 km/Ma rate across Sinaloa and the central Sierra Madre Occidental.

These variations in distance and rate of migration along the magmatic arc were not considered in earlier interpretations about patterns of arc magmatism in México and the southwestern United States. An eastward progression of magmatism was first well established for the southwestern United States and northwestern México (Anderson and Silver, 1974; Coney and Reynolds, 1977; Silver et al., 1979; Damon et al., 1981; Silver and Chappell, 1988; Ortega-Rivera, this volume, Chapter 11). For example, Damon et al. (1981) extrapolated age information from a 1200-km-long, arc-parallel swath from the U.S. border to the Trans-Mexican volcanic belt onto a single east-northeast reference line (Fig. 10C). Their included arc length is greater than the length of their cross-arc traverse. By combining data from near the México-U.S. border, where magmatism migrated far inland, and from the Sinaloa-Durango area, where magmatism did not, the compilation of Damon et al. (1981) gives the impression that magmatism migrated far inland throughout México. Their compilation includes our data from southern Sinaloa, yet it yields markedly different results than we derive for our data alone.

We do not know the location of the change from the long and rapid migration of magmatism in northern and southern México to the much slower and shorter migration in Sinaloa, or whether the change is gradational or abrupt. The zone of shorter migration approximately coincides with the Guerrero or Tahue terrane, which is composed of possibly accreted rocks that are no older than Jurassic (Campa and Coney, 1983; Coney and Campa, 1987; Sedlock et al., 1993; Tardy et al., 1994). Our data and published work (e.g., Ortega-Rivera, this volume, Chapter 11) require that the northern change be north of north-central Sinaloa and south of central Sonora, a location that approximately coincides with the southern edge of North American Proterozoic basement (Fig. 1; Valencia-Moreno et al., 2001). The location between Sinaloa and Jalisco-Oaxaca is even less certain. However, the basement in Jalisco is Jurassic(?) metasedimentary rock (Gastil et al., 1978), similar to basement in Sinaloa, whereas Precambrian metamorphic rocks are encountered in the middle and eastern parts of the Jalisco–Oaxaca trend (Centeno-Garcia et al., 1993; Schaaf et al., 1995). A very speculative possibility is that the character of the overriding plate influenced the pattern of subduction. Rapid subduction has been suggested as the cause of the eastward migration of magmatism (Hamilton, 1988), but rapid subduction occurred along the whole length of northwestern México, so that cannot be the only factor (Engebretson et al., 1985; Stock and Molnar, 1988).

Arc Migration and Plate Tectonics

A detailed analysis of the relationship between arc migration and regional plate tectonic history is beyond the scope of this paper. Many authors (e.g., Hamilton, 1988) have suggested that the position of a magmatic arc relative to its convergent margin (the arc-trench gap) is a function of the dip angle of the subducting plate, which in turn is related to the orthogonal rate of plate convergence. Analysis of changes in the arc position generally assumes a uniform dip angle for the entire length of the slab and a similar depth range for the first stage of magma production. These conditions predict a regular migration of the arc through time and an increase in the width of the arc away from the trench. However, the actual magmatic record for the Cordillera of North America is anything but uniform. The abrupt drop-off of Late Cretaceous–early Tertiary igneous activity eastward from the Sierra Nevada batholith, and the Eocene-Oligocene ignimbrite flare-ups of the western United States—and especially the Sierra Madre Occidental—are two examples of the episodic nature of magma production in time and space. Hence, as indicators of subduction history, compilations of age versus location are incomplete indicators without attempts to assess variations in the rate of magma production through time. Moreover, most existing compilations for the Late Cretaceous–

early Tertiary magmatic history of western North America have failed to include data for the "coeval" volcanic rocks, which can provide a critical part of a region's magmatic history (McDowell et al., 2001). Indeed, the lower volcanic complex remains undated in Sinaloa. Finally, the order of magnitude contrast between the migration rate calculated for the magmatic arc of Baja-Sonora and that of Sinaloa requires significant contrasts in subduction pattern along the Farallon–North America plate margin.

Ties across the Gulf of California

Both granitic and volcanic rocks of Sinaloa are similar to those of the east coast of Baja California Sur, which lay adjacent to Sinaloa before transform opening of the Gulf of California. Based on reconstructions by Stock and Hodges (1989), Mazatlan lay approximately opposite La Paz, and our northern transect lay between Loreto and Bahia Concepcion (Fig. 11), rare locations where granitic rocks are exposed in Baja California Sur north of La Paz. As discussed above, the granitic rocks of the Cabo San Lucas block are similar to those of Sinaloa (Frizzell et al., 1984; Hausback, 1984; Aranda-Gómez and Perez-Venzor, 1989; Kimbrough et al., 2002). A slightly lineated, mafic quartz diorite dated at 87.4 ± 2.0 Ma (K-Ar, biotite; McLean, 1988) crops out just northwest of Loreto. The rock type and age are indistinguishable from those of the syntectonic rocks of Sinaloa. Host rocks for the quartz diorite are greenschist facies volcaniclastic sandstone and conglomerate, probably similar to rocks described by Bonneau (1970) in our northern transect but only somewhat like the metasedimentary rocks of southern Sinaloa. McFall (1968) reports "granodiorite to quartz monzonite" with a 80.4 ± 2.8 Ma biotite age at Bahia Concepcion.

Miocene volcanic and intrusive rocks are also similar along the east coast of Baja California Sur and in Sinaloa. In an extensive study of volcanism in and north of La Paz, Hausback (1984) reports volcanic rocks ranging from 28 to 12 Ma. Rocks from ca. 24 to 12 Ma include rhyolitic ash-flow tuffs and andesite to rhyodacite lavas erupted from sources in Baja California. Rhyolitic tuffs with ages between 28 and 24 Ma appear to have erupted from sources east of Baja California, presumably in either Sinaloa or Durango. McLean (1988) reports 22 Ma ages on two ash-flow tuffs and a 19 Ma hornblende andesite intrusion near Loreto, and McFall (1968) reports a 29 Ma ash-flow tuff and a 20.5 Ma tonalite stock near Bahia Concepcion.

Although these similarities support matching southern Sinaloa across the Gulf of California to the area between La Paz and Loreto, it must be noted that similar rocks occur all along the length of the former Cordilleran arc. More distinct rock types need to be correlated (Gastil et al., 1981; Oskin et al., 2001), because the general character of rocks is not diagnostic. Ash-flow tuffs of the upper volcanic sequence are probably the most promising for correlation. They are known to crop out on both sides of the Gulf, individual tuffs would have been sufficiently widespread to extend across the now separated terranes, and highly precise methods such as $^{40}Ar/^{39}Ar$ dating are available for correlation.

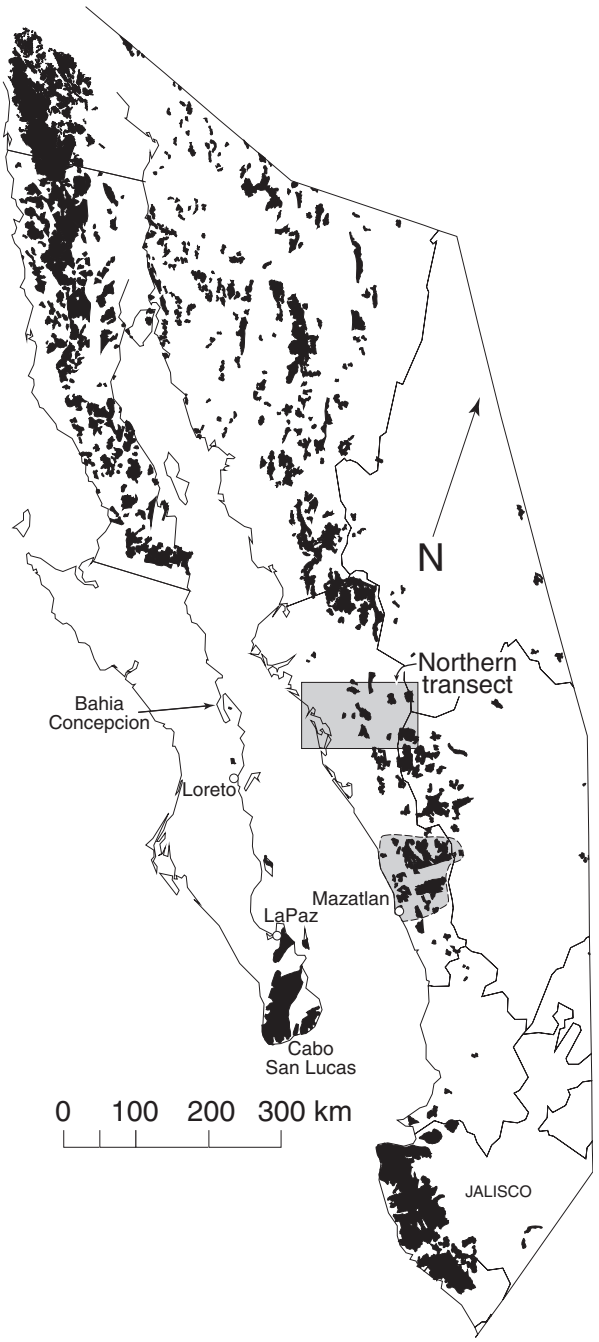

Figure 11. Baja California restored to its position relative to mainland México before transform faulting that began ca. 6 Ma but after Miocene, east-northeast extension that began ca. 12 Ma (adapted from Stock and Hodges, 1989). Mazatlan lay opposite La Paz and north of Cabo San Lucas block. Our northern transect lay between Loreto and Bahia Concepcion. Miocene extension affected area between eastern edge of Baja California and western edge of Sierra Madre Occidental and also east of Sierra Madre (Henry and Aranda-Gómez, 2000). Before this extension, Cabo San Lucas batholith may have lain more closely between batholiths of southern Sinaloa and Jalisco (Schaaf et al., 1997, 2000; Moran-Zenteno et al., 2000).

ACKNOWLEDGMENTS

We thank Goran Fredrikson, Steve Clabaugh, Michel Bonneau, and Ken Clark for discussions about the geology of Sinaloa and Jim Faulds for discussions about the character and significance of dynamic recrystallization textures. Geologists and staff of Minas de San Luis, now Luismin, provided hospitality, a place to stay, and a thorough knowledge of the geology around Tayoltita, in the northeastern part of the area. Paul Guenther provided instruction and guidance during K-Ar dating; Thomas Anderson, Jaime Alvarez, and Gerri Silver did the same for U-Pb work. The opportunity for this study arose through a project of the Instituto de Geologia, Universidad Nacional Autónoma de México, funded by the state of Sinaloa. The project provided expenses, vehicles, and other supplies during 1971 and 1972. Funds were also provided by a Penrose Research Grant from the Geological Society of America and by National Science Foundation Grant GA-16080 to Steve Clabaugh. We also thank Stan Keith for providing many of the chemical analyses reported here and Mark Barton and Joaquin Ruiz for providing the data to construct the map of granitic rocks in western México. Finally, we thank Jim Mattinson and David Kimbrough for helpful, constructive reviews.

APPENDIX 1: DATING PROCEDURES

Both K-Ar and U-Pb dating were done in the early 1970s using procedures and instruments of that time.

K-Ar Procedures

Samples for K-Ar dating were crushed and ground and a 60–80 mesh fraction was used for mineral separation. Biotite and hornblende were separated using standard magnetic and heavy liquid techniques. K analyses were done with a Baird-Atomic model KY-2 flame photometer using a Li internal standard and Na buffering. Approximately 100 mg aliquots were dissolved with HF, HCL, and HNO_3, dried and redissolved twice with HCL to get rid of fluoride ions, and then taken up with HCl and deionized H_2O. Final solutions were made to have K concentrations of less than 8 ppm.

Ar analysis was done in an on-line extraction system where the furnace, purification system, ^{38}Ar spike and calibration system, and mass spectrometer are part of one vacuum system. Approximately 100 mg of biotite and 500 mg of hornblende were spiked and then melted in a Mo crucible at ~1700 °C using a RF induction heater. The released gas was purified, passed through a series of zeolite traps and Ti getters. Isotopic analysis was done on a CEC 21–615 cycloidal focusing residual gas analyzer operated in the static mode.

Pooled standard deviations for K content were 0.61% and 1.14% and for Ar content 0.95% and 1.97% for biotite and hornblende, respectively. These values combine to give an estimated analytical precision of 1.13% and 2.28% for biotite and hornblende ages, which have been applied here.

U-Pb Procedures

Crushed and ground samples were passed across a Wilfley table and further concentrated with a hand magnet and heavy liquids. The sample was sieved, and the various size fractions were run through a magnetic separator. The least magnetic material was washed with hot HNO_3 and rerun through the magnetic separator. Resulting zircon fractions have been demonstrated to show a correlation between U content, magnetic susceptibility, and size, with the most magnetic and smallest zircons having the highest U content (Silver, 1963).

Separate aliquots of ~200–400 mg of each zircon size-magnetic susceptibility fraction were fused with a borate flux and analyzed for U and Pb concentration and Pb isotopic composition. The concentration aliquot was spiked with ^{208}Pb and ^{235}U before fusion. Pb purification for each aliquot was done by double dithizone extraction. Purified Pb was picked up in silica gel and loaded on a single Re filament. U purification was done by anion exchange. U was picked up in HNO_3 and loaded on a single Ta filament. Mass spectrometry was performed on a 60° sector field, single-focusing instrument with a 12-in (30.5 cm) radius of curvature.

Observed Pb isotope ratios were corrected for both blank and natural common Pb using $^{206}Pb/^{204}Pb = 18.60$ and $^{207}Pb/^{204}Pb = 15.60$. Borate flux was the major source of blank Pb and constituted most of the ^{207}Pb in almost all analyses.

REFERENCES CITED

Aguirre-Díaz, G.J., and McDowell, F.W., 1991, The volcanic section at Nazas, Durango, México, and the possibility of widespread Eocene volcanism within the Sierra Madre Occidental: Journal of Geophysical Research, v. 96, p. 13,373-13,388.

Anders, E., and Grevesse, N., 1989, Abundances of the elements: Meteoritic and solar: Geochimica et Cosmochimica Acta, v. 53, p. 197–214.

Anderson, T.H., and Silver, L.T., 1974, Late Cretaceous plutonism in Sonora, México, and its relationship to Circum-Pacific magmatism: Geological Society of America Abstracts with Programs, v. 6, p. 484.

Aranda-Gómez, J.J, Henry, C.D., Luhr, J.F., and McDowell, F.W., 1997. Cenozoic volcanism and tectonics in NW México—A transect across the Sierra Madre Occidental volcanic field and observations on extension related magmatism in the southern Basin and Range and Gulf of California tectonic provinces, *in* Aguirre-Díaz, G.J., Aranda-Gómez, J.J., Carrasco-Nuñez, G., and Ferrari, L., eds., Magmatism and tectonics in the central and northwestern México—A selection of the 1997 IAVCEI General Assembly excursions: Universidad Nacional Autónoma México, Instituto de Geologia, México, D.F., Excursión 11, 41–84.

Aranda-Gómez, J.J., and Perez-Venzor, J.A., 1989, Estratigrafia del complejo cristalino de la region de Todos Santos, Estado de Baja California Sur: Revista de Universidad Nacional Autónoma de México, Instituto de Geologia, v. 8, p. 149–170.

Baird, A.K., and Miesch, A.T., 1984, Batholithic rocks of Southern California—A model for the petrochemical nature of their source materials: U.S. Geological Survey Professional Paper 1284, 42 p.

Bateman, P.C., 1992, Plutonism in the central part of the Sierra Nevada Batholith, California: U.S. Geological Survey Professional Paper 1483, 186 p.

Bonneau, M., 1970, Una nueva area Cretacica fosilifera en el estado de Sinaloa: Boletin Sociedad Geologica Mexicana, v. 32, p. 159-167.

Campa, M.F., and Coney, P.J., 1983, Tectono-stratigraphic terranes and mineral resource distributions in México: Canadian Journal of Earth Sciences, v. 20, p. 1040–1051.

Cibula, D.A., 1975, The geology and ore deposits of the Cosala mining district, Cosala municipality, Sinaloa, México: [M.S. thesis]: University of Iowa, 145 p.

APPENDIX 2. SAMPLE DESCRIPTIONS AND LOCATIONS

Sample	Rock name (granitic type)	Location and type of outcrop	Mineralogy
HM-1	Rhyodacite flow (upper volcanic sequence)	Roadcut on Highway 40 8 km northeast of Villa Union	30% plagioclase, 5% biotite and 2% quartz phenocrysts in groundmass of quartz, alkali feldspar, and plagioclase
HM-4	Mafic tonalite (Recodo)	Outcrop in stream bed 7 km southwest of Rocodo	53% plagioclase, 16% quartz, 6% microcline, 14% biotite, 11% hornblende
HM-8	Mafic tonalite	Erosional remnant 7 km east of San Marcos	52% plagioclases 21% quartz, 4% microcline, 14% biotite, 13% hornblende
HM-9	Monzogranite	Outcrop in stream bed 8 km east of San Marcos	33% plagioclase, 19% quartz, 41% orthoclase, 6% biotite
HP-2	Granodiorite (San Ignacio)	Erosional remnant 7 km east of Ixpalino	39% plagioclase, 27% quartz, 17% orthoclase, 9% biotite, 7% hornblende
HP-4	Quartz diorite	Outcrop in stream bed in Ixpalino	61% plagioclase, 13% quartz, 10% biotite, 11% hornblende, 3% pyroxene, 3% opaques
HP-5	Granodiorite	Erosional remnant 8.5 km north of Elota	51% plagioclase, 21% quartz, 16% orthoclase, 7% biotite, 5% hornblende
HP-6	Granodiorite (Candelero)	Roadcut on Highway 15, 2 km west of Elota	55% plagioclase, 20% quartz, 9% orthoclase, 8% biotite, 8% hornblende
HP-7	Quartz diorite	Erosional remnant 10 km north of San Ignacio	71% plagioclase, 7% quartz, 22% hornblende and clinopyroxene
HP-10	Andesite dike (upper volcanic sequence)	Outcrop in stream bed 12 km north of San Ignacio	7% hornblende, 4% altered plagioclase phenocrysts in groundmass of plagioclase, hornblende and opaques
HP-11	Granodiorite (San Ignacio)	Erosional remnant 6 km east of San Ignacio	43% plagioclase, 24% quartz, 19% orthoclase, 9% biotite, 5% hornblende
HP-13	Monzogranite (Candelero)	Roadcut 6 km east of San Juan	37% plagioclase, 34% orthoclase, 27% quartz, 4% biotite, 2% hornblende
HP-14	Granodiorite (Candelero)	Outcrop in stream bed near Candelero	47% plagioclase, 22% quartz, 18% orthoclase, 8% biotite, 3% hornblende
HP-15	Granodiorite	Outcrop in stream bed 4 km south of Pueblo Viejo	47% plagioclase, 24% quartz, 15% microcline, 11% biotite, 4% hornblende
HP-16	Granodiorite	Stream bed 4 km northeast of Pueblo VieJo	41% plagioclase, 22% quartz, 17% orthoclase, 11% biotite, 9% hornblende
HP-18	Granodiorite (Candelero)	Outcrop in Rio Piaxtla 10 km northeast of Tayoltita	46% plagioclase, 26% quartz, 19% orthoclase, 8% biotite, 1% hornblende
HP-20	Granodiorite (Candelero)	Outcrop in stream bed 18 km northeast of Tayoltita	46% plagioclase, 25% quartz, 14% orthoclase, 8% biotite, 4% hornblende
HP-22	Granodiorite	Outcrop in stream bed 12 km northeast of Tayoltia	51% plagioclase, 19% quartz, 11% orthoclase, 10% biotite, 7% hornblende
HP-23	Granodiorite (Candelero)	Outcrop in Arroyo Chicaral 9 km east of Tayoltita	59% plagioclase, 22% quartz, 14% orthoclase, 5% biotite
HP-24	Quartz diorite dike (upper volcanic sequence)	Outcrop in Arroyo San Geronimo 9 km northeast of Tayoltita	67% plagioclase, 15% biotite, 10% hornblende, 8% quartz
HP-25	Granodiorite (Candelero)	Outcrop in Arroyo 8 km west of Tayoltita	56% plagioclase, 17% quartz, 14% orthoclase, 9% biotite, 2% hornblende
HP-26	Granodiorite (San Ignacio)	Outcrop in Rio Piaxtla 4 km southwest of Tayoltita	40% plagioclase, 25% quartz, 20% orthoclase, 10% biotite, 5% hornblende
HP-28	Granodiorite (Candelero)	Outcrop in Rio Piaxtla 8 km southwest of Tayoltita	46% plagioclase, 25% quartz, 22% orthoclase, 6% biotite, l% hornblende

(continued)

APPENDIX 2. SAMPLE DESCRIPTIONS AND LOCATIONS *(continued)*

Sample	Rock name (granitic type)	Location and type of outcrop	Mineralogy
HS-8B	Porphyritic granodiorite (Concordia)	Roadcut on Highway 40, 5 km west of Concordia	43% Plagioclase, 20% quartz, 21% orthoclase as l cm porphyroblasts, 6% biotite, 10% hornblende
HS-12	Granodiorite (El Carmen)	Roadcut on San Ignacio Road	50% plagioclase, 25% quartz, 10% orthoclase, 8% biotite, 7% hornblende (with pyroxene cores)
HS-13	Granodiorite (El Carmen)	Roadcut on San Ignacio Road	45% plagioclase, 25% quartz, 15% orthoclase) 10% biotite, 5% hornblende
HS-15	Granodiorite	Roadcut on San Ignacio Road	50% plagioclase, 25% quartz, 15% orthoclase, 7% biotite, 3% hornblende (with pyroxene cores)
HS-17	Mafic tonalite (Recodo)	Outcrop in stream bed 2 km southwest of Recodo	60% plagioclase, 14% quartz, 1% Kfeldspar, 10% biotite, 15% hornblende (with pyroxene cores)
HS-22	Foliated tonalite	Erosional remnant 2 km southwest of San Marcos	54% plagioclase, 16% quartz, 13% biotite, 5% microcline, 12% hornblende (with Py.roxene cores)
HS-23	Granodiorite	Outcrop in stream bed near Rio Presidio, 5 km east of San Marcos	40% plagioclase, 30% quartzi 20% orthoclase, 6% biotite, 4% hornblende
HS-25	Porphyritic granodiorite (El Carmen)	Roadcut on dirt road 8 km east of Coyotitan	45% plagioclase (some as porphyroblasts up to 2 cm long), 35% quartz, 10% orthoclase, 7% biotite, 3% hornblende
HS-32	Hypersthene granodiorite	Erosional remnant 6 km west of La Noria	55% plagioclase, 15% hypersthene-, 12% biotite, 10% quartz, 8% orthoclase
HS-34	Foliated granodiorite	Erosional remnant 4.km northwest of Quelite	48% plagioclase, 25% quartz, 6% biotite, 8% microcline, 13% hornblende
HS-37	Foliated granodiorite	Outcrop in jungle 10 km south of La Cruz	40% plagioclase, 23% quartz, 18% biotite, 8% hornblende (with rare cores of pyroxene), 11% microcline
HS-40	Tonalite (San Ignacio border phase)	Outcrop in stream bed near San Javier	50% plagioclase, 40% quartz, 9% biotite, 1% hornblende
HS-4l	Quartz diorite (San Ignacio border phase)	Outcrop in stream bed near San Javier (same as HS-40)	70% plagioclase, 20% biotite, 10% quartz
HS-42	Granodiorite (San Ignacio)	Outcrop in bed of Rio Piaxtla across from San Ignacio	43% plagioclase, 27% quartz, 15% orthoclase, 9% biotite, 6% hornblende (cores of pyroxene)
HS-43	Amphibolite (possible metadiorite?)	Outcrop in stream bed 5 km north of San Marcos	50% plagioclase, 40% hornblende, 5% quartz, 1% biotite
HS-44	Tonalite	Erosional remnant 1 km west of Highway 15 near Quelite	55% plagioclase, 27% quartz, 15% biotite, 3% microcline
HS-45	Gneissic tonalite (Quelite tonalite)	Quarry along road to Marmol	55% plagioclase, 20% quartz, 12% biotite, 11% hornblende, 2% microcline
HS-46	Hornblende gabbro	Roadcut 6 km southwest of La Noria	70% plagioclase, 15% hornblende, 15% fibrous alteration
HS-48	Hornblende gabbro	Outcrop in stream bed 3 km north of Cofradia	60% plagioclase 30% hornblende, 7% alteration, 3% quartz
HS-49	Tonalite	Roadcut 7 km northeast of El Verde	66% plagioclase, 25% quartz, 5% biotite, 3% orthoclase, 1% hornblende and clinopyroxene
HS-50	Tonalite	Outcrop in stream bed 1 km south of Naranjos	50% plagioclase, 30% quartz, 10% biotite, 5% hornblende, 2% orthoclase
HS-51	Granodiorite	Outcrop in stream bed at Panuco	40% quartz, 35% plagioclase, 10% orthoclase, 10% biotite
HS-53	Tonalite (Colegio tonalite)	Erosional remnant 9 km north of Quelite	60% plagioclase, 14% quartz, 2% orthoclase, 11% biotite, 13% hornblende
146	Granodiorite (San Ignacio)	Outcrop in Rio Piaxtla 1.5 km north of Los Brasiles	48% plagioclase, 20% quartz, 11% orthoclase, 13% biotite, 8% hornblende

(continued)

APPENDIX 2. SAMPLE DESCRIPTIONS AND LOCATIONS *(continued)*

Sample	Rock name (granitic type)	Location and type of outcrop	Mineralogy
152	Granodiorite	Outcrop in Rio Piaxtla 7 km southwest of Los Brasiles	50% plagioclase, 20% quartz, 8% orthoclase, 10% biotite, 11% hornblende
156	Granodiorite (San Ignacio)	Outcrop in Rio Piaxtla 11 km east of San Ignacio	42% plagioclase, 21% quartz, 20% orthoclase, 9% biotite, 7% hornblende
170	Monzogranite (San Ignacio)	Outcrop in Rio Piaxtla 11 km east-northeast of San Ignacio	44% plagioclase, 18% quartz, 24% orthoclase, 6% biotite, 7% hornblende
174	Rhyolite dike	Outcrop in stream bed 3 km southwest of Ajoya	2% biotite and 1% plagioclase phenocrysts in groundmass of plagioclase, quartz, K feldspar and biotite
199	Tonalite	Outcrop in Rio Piaxtla 8 km southwest of Los Brasiles	69% plagioclase, 15% quartz, 8% biotite, 5% hornblende and clinopyroxene, 3% orthoclase
227	Granodiorite	Outcrop in Rio Verde 6.5 km north of Ajoya	55% plagioclase, 12% quartz, 14% orthoclase, 16% biotite, 3% hornblende
230	Granodiorite	Outcrop in Arroyo Verano near Verano north of map area	49% plagioclase, 16% quartz, 13% orthoclase, 15% biotite, 8% hornblende
236	Monzogranite (Candelero)	Quarry in Ajoya	37% plagioclase, 26% quartz, 26% orthoclase, 5% biotite, 6% hornblende
GD	Granodiorite	Mine workings at Tayoltita	56% plagioclase, 20% quartz, 20% orthoclase, 4% biotite
Hbl	Porphyritic granodiorite	Mine workings at Tayoltita	1% hornblende phenocrysts in highly altered groundmass of plagioclase, opaques, and quartz
Adul	Adularia-bearing vein	Mine Workings at Tayoltita	quartz, adularia, and calcite filling vein in andesite
HC-3	Granodiorite (Candelero)	Erosional remnant 15 km northwest of Badiraguato, northern Sinaloa	55% plagioclase, 24% quartz, 7% orthoclase, 10% biotite, 4% hornblende
HC-4	Mafic foliated tonalite	Outcrop in stream bed 20 km north of Pericos, northern Sinaloa	50% plagioclase, 20% biotite, 15% quartz, 10% hornblende, 5% microcline
HC-5	Granodiorite	Erosional remnant 10 km north of HC-4, northern Sinaloa	50% plagioclase, 25% quartz, 10% orthoclase, 10% biotite, 5% hornblende
HC-6	Monzogranite	Outcrop in stream bed 10 km east of Presa Adolfo L. Mateos, northern Sinaloa	35% plagioclase, 25% quartz, 25% orthoclase, 8% biotite, 7% hornblende
KC-1	Granodiorite	13 km east of Villa Union near Malpica	quartz, plagioclase, orthoclase, biotite, hornblende
KC-2	Gneissic Granodiorite	5 km southwest of Tabora, northern Sinaloa	49% plagioclase, 21% quartz, 13% microcline, 7% biotite, 8% hornblende
KC-3	Monzogranite	2 km east of Tameapa, northern Sinaloa	30% plagioclase, 20% quartz, 40% orthoclase, 10% biotite and altered hornblende

Clarke, M., and Titley, S.R., 1988, Hydrothermal evolution in the formation of silver-gold veins in the Tayoltita Mine, San Dimas District: Economic Geology, v. 83, p.1830–1840.

Coney, P.J., and Campa, M.F., 1987, Lithotectonic terrane map of Mexico (west of the 91st meridian): U.S. Geological Survey Miscellaneous Field Studies Map MF-1874-D, scale 1:2,500,000, 1 sheet.

Coney, P.J., and Reynolds, S.J., 1977, Cordilleran Benioff zones: Nature, v. 270, p. 403- 406.

Damon, P.E., Shafiqullah, M., and Clark, K.F., 1981, Age trends of igneous activity in relation to metallogenesis in the southern Cordillera: Arizona Geological Society Digest, v. 14, p. 137-154.

Damon, P.E., Shafiqullah, M., and Clark, K.F., 1983a, Geochronology of the porphyry copper deposits and related mineralization of México: Canadian Journal of Earth Science, v. 20, p. 1052–1071.

Damon, P.E., Shafiqullah, M., Roldan, J., and Cocheme, J.J., 1983b, El batolito Laramide (90–40 Ma) de Sonora: Asociacion de Ingenieros de Minas, Metalurgistas y Geologos de México, A.C., Memoria, XV Convencion Nacional, p. 63–95.

Damon, P.E., Shafiqullah, M., and Roldan-Quintana, J., 1984, The Cordilleran Jurassic arc from Chiapas (southern Mexico) to Arizona: Geological Society of America Abstracts with Programs, v. 16, no. 6, p. 482.

Engebretson, A.C., Cox, A., and Gordon, R.G., 1985, Relative motions between oceanic and continental plates in the Pacific Basin: Boulder, Colorado, Geological Society of America Special Paper 206, 59 p.

Evernden, J.F., and Kistler, R.W., 1970, Chronology of emplacement of Mesozoic batholithic complexes in California and western Nevada: U.S. Geological Survey Professional Paper 623, 42 p.

Ferrari, L., Pasquare, G., Venegas-Salgado, S., and Romero-Rios, F., 2000, Geology of the western Mexican volcanic belt and adjacent Sierra Madre

Occidental and Jalisco Block: Boulder, Colorado, Geological Society of America Special Paper 334, p. 65–83.
Frizzell, V.A, Jr., 1984, The geology of the Baja California peninsula; An introduction, *in* Frizzell, V.A., Jr., ed., Geology of the Baja California Peninsula: Los Angeles, Society of Economic Paleontologists and Mineralogists Pacific Section, v. 39, p. 1–7.
Frizzell, V.A, Jr., Fox, L.K., Moser, F.C., and Ort, K.M., 1984, Late Cretaceous granitoids, Cabo San Lucas Block, Baja California Sur, México: Eos (Transactions, American Geophysical Union), v. 65, p.1151
Gans, P.B., 1997, Large-magnitude Oligo-Miocene extension in southern Sonora: implications for the tectonic evolution of northwest México: Tectonics, v. 16, p. 388–408.
Gastil, R.G., 1975, Plutonic zones in the Peninsular Ranges of southern California and Baja California: Geology, v. 3, p. 361–363.
Gastil, R.G., and Krummenacher, D., 1977, Reconnaissance geology of coastal Sonora between Puerto Lobos and Bahia Kino: Geological Society of America Bulletin, v. 88, p. 189-198.
Gastil, R.G., Phillips, R.P., and Allison, E.C., 1975, Reconnaissance geology of the state of Baja California: Boulder, Colorado, Geological Society of America Memoir 140, 170 p.
Gastil, R.G., Krummenacher, D., and Jensky, W.E., 1978, Reconnaissance geologic map of the west-central part of Nayarit, México: Geological Society of America, Map and Chart Series Map MC-24, scale 1:200,000, 1 sheet.
Gastil, R.G., Krummenacher, D., and Minch, J., 1979, The record of Cenozoic volcanism around the Gulf of California: Geological Society of America Bulletin, v. 90, p. 839-857.
Gastil, R.G., Morgan, G.J., and Krummenacher, D., 1981, The tectonic history of peninsular California and adjacent México, *in* Ernst, W.G., ed., The geotectonic development of California, Rubey Volume I: Englewood Cliffs, New Jersey, Prentice-Hall, p. 284–305.
Gromet, L.P., and Silver, L.T., 1987, REE variations across the Peninsular Ranges batholith: Implications for batholithic petrogenesis and crustal growth in magmatic arcs: Journal of Petrology, v. 28, p. 75–125.
Hamilton, W., 1988, Tectonic setting and variations with depth of some Cretaceous and Cenozoic structural and magmatic systems of the western United States, *in* Ernst, W.G., ed., Metamorphism and crustal evolution of the western United States, Rubey Volume VII: Englewood Cliffs, New Jersey, Prentice-Hall, p. 1–40.
Harrison, T.M., 1981, Diffusion of ^{40}Ar in hornblende: Contributions to Mineralogy and Petrology, v. 78, p. 324-331.
Harrison, T.M., Duncan, I., and McDougall, I., 1985, Diffusion of ^{40}Ar in biotite; temperature, pressure and compositional effects: Geochimica et Cosmochimica Acta, v. 49, p. 2461–2468.
Hausback, B.P., 1984, Cenozoic volcanic and tectonic evolution of Baja California Sur, México, *in* Frizzell, V.A., Jr., ed., Geology of the Baja California peninsula: Los Angeles, Society of Economic Paleontologists and Mineralogists Pacific Section, v. 39, p. 219-236.
Henry, C.D., 1989, Late Cenozoic Basin and Range structure in western México adjacent to the Gulf of California: Geological Society of America Bulletin, v. 101, p. 1147–1156.
Henry, C.D., and Aranda-Gómez, J.J., 2000, Plate interactions control middle-late Miocene, proto-Gulf and Basin and Range extension in the southern Basin and Range: Tectonophysics, v. 318, p. 1–26.
Henry, C.D., and Fredrikson, G., 1987, Geology of southern Sinaloa adjacent to the Gulf of California: Geological Society of America, Map and Chart Series, Map MCH063, 1 sheet.
Henry, C.D., Price, J.G., and James, E.W., 1991, Mid-Cenozoic stress evolution and magmatism in the southern Cordillera, Texas and México: Transition from continental arc to intraplate extension: Journal of Geophysical Research, v. 96, p. 13545–13560.
Holguin, Q.N., 1978, Estudio estratigrafico del Cretacico inferior en el norte de Sinaloa, México: Revista del Instituto Mexicano del Petroleo, January 1978, p. 6–13.
Housh, T., and McDowell, F.W., 1999, Delineation of basement provinces in northwestern México through isotopic studies of late-Cretaceous to mid-Tertiary igneous rocks [abs.]: Eos (Transactions, American Geophysical Union), v. 80, p. F987.
Jennings, C.W., compiler, 1977, Geologic map of California: California Division of Mines and Geology, Geologic Data Map No. 2, scale: 1:750,000, 1 sheet**]**.
Johnson, S.E., Paterson, S.R., and Tate, M.C., 1999a, Structure and emplacement history of a multiple-center, cone-sheet-bearing ring complex: The Zarza intrusive complex, Baja California, México: Geological Society of America Bulletin, v. 111, p. 607–619.
Johnson, S.E., Tate, M.C., and Fanning, C.M., 1999b, New geologic mapping and SHRIMP U-Pb zircon data in the Peninsular Ranges Batholith, Baja California, México: Evidence for a suture?: Geology, v. 27, p. 743–746.
Kimbrough, D.L., Smith, D.P., Mahoney, J.B., Moore, T.E., Grove, M., Gastil, R.G., Ortega-Rivera, A., Fanning, C.M., 2001, Forearc-basin sedimentary response to rapid Late Cretaceous batholith emplacement in the Peninsular Ranges of Southern and Baja California: Geology, v. 29, p. 491–494.
Kimbrough, D.L., Gastil, R.G., Garrow, P.K., Grove, M., Aranda-Gómez, J.J., Perez-Venzor, J.A., and Fletcher, J., 2002, A potential correlation of plutonic suites from the Los Cabos block and Peninsular Ranges batholith: VI International Meeting on Geology of the Baja California Peninsula, La Paz, Baja California Sur: Universidad Autónoma de Baja California, p. 9.
Lipman, P.W., 1984, The roots of ash flow calderas in western North America: Windows into the tops of granitic batholiths: Journal of Geophysical Research, v. 89, p. 8801–8841.
Krummenacher, D., Gastil, R.G., Bushee, J., and Doupont, J., 1975, K-Ar apparent ages, Peninsular Ranges batholith, southern California and Baja California: Geological Society of America Bulletin, v. 86, p. 760–768.
Martiny, B., Martinez Serrano, R.G., Moran Zenteno, D.J., Macias Romo, C., and Ayuso, R.A., 2000, Stratigraphy, geochemistry and tectonic significance of the Oligocene magmatic rocks of western Oaxaca, southern México: Tectonophysics, v. 318, p. 71–98.
McDowell, F.W., and Clabaugh, S.E., 1979, Ignimbrites of the Sierra Madre Occidental and their relation to the tectonic history of western México: Boulder, Colorado, Geological Society of America Special Paper 180, p. 113–124.
McDowell, F.W., and Keizer, R.P., 1977, Timing of mid-Tertiary volcanism in the Sierra Madre Occidental between Durango City and Mazatlan, México: Geological Society of America Bulletin, v. 88, p. 1479-1486.
McDowell, F.W., and Mauger, R.L., 1994, K-Ar and U-Pb zircon chronology of Late Cretaceous and Tertiary magmatism in central Chihuahua state, México: Geological Society of America Bulletin, v. 106, p. 118–132.
McDowell, F.W., Roldan-Quintana, J., and Connelly, J.N., 2001, Duration of Late Cretaceous–early Tertiary magmatism in east-central Sonora, México: Geological Society of America Bulletin, v. 113, p. 521–531.
McFall, C.C., 1968, Reconnaissance geology of the Concepcion Bay area, Baja California, México: Stanford, Stanford University, Geological Sciences, v. 10, no. 5, 25 p.
McLean, H., 1988, Reconnaissance geologic map of the Loreto and part of the San Javier quadrangles, Baja California Sur, México: U.S. Geological Survey Miscellaneous Field Studies Map MF-2000, scale 1:50,000, 1 sheet.
Mora-Alvarez, G., and McDowell, F.W., 2000, Miocene volcanism during late subduction and early rifting in the Sierra Santa Ursula of western Sonora, México, *in* Delgado-Granados, H., Aguirre-Díaz, G., and Stock, J.M., eds., Cenozoic tectonics and volcanism of México: Boulder, Colorado, Geological Society of America Special Paper 334, p. 123–141.
Moran-Zenteno, D.J., Martiny, B., Tolson, G., Solis-Pichardo, G., Alba-Aldave, L., Hernandez-Bernal, M.D.S., Macias-Romo, C., Martinez-Serrano, R.G., Schaaf, P., and Silva-Romo, G., 2000, Geocronologia y caracteristicas geoquimicas de las rocas magmaticas terciarias de la Sierra Madre del Sur: Boletin de la Sociedad Geologica Mexicana, v. 53, p. 27–58.
Mullan, H.S., 1978, Evolution of part of the Nevadan orogen in northwestern México: Geological Society of America Bulletin, v. 89, p. 1175-1188.
Nemeth, K.E., 1976, Petrography of the Lower Volcanic group, Tayoltita–San Dimas district, Durango, México [M.A. thesis]: Austin, The University of Texas, 141 p.
Nieto-Samaniego, A.F., Ferrari, L., Alaniz-Alvarez, S.A., Labarthe-Hernández, G., and Rosas-Elguera, R., 1999, Variation of Cenozoic extension and volcanism across the southern Sierra Madre Occidental volcanic province, México: Geological Society of America Bulletin, v. 111, p. 347–363.
Ortega-Gutiérrez, F., Prieto-Velez, R., Zuniga, Y., and Flores, S., 1979, Una secuencia volcano-plutonica-sedimentaria Cretacica en el norte de Sinaloa; un complejo ofiolitico?: Revista de Universidad Nacional Autónoma de México, Instituto de Geologia,, v. 3, p.1–8.
Ortega-Gutiérrez, F., Mitre-Salazar, L.M., Roldan-Quintana, J., Aranda-Gómez, J., Moran-Zenteno, D., Alaniz-Alvarez, S., and Nieto-Samaniego, A., 1992, Carta geologica de la Republica Mexicana: Instituto de Geologia, Universidad Nacional Autónoma de México, scale 1:2,000,000, 1 sheet.
Ortega-Rivera, A., Farrar, E., Hanes, J.A., Archibald, D.A., Gastil, R.G., Kimbrough, D.L., Zentilli, M., Lopez-Martinez, M., Feraud, G., and Ruffet, G., 1997, Chronological constraints on the thermal and tilting history of the Sierra San Pedro Martir pluton, Baja California, México, from U/Pb, ^{40}Ar/^{39}Ar, and fission-track geochronology: Geological Society of America Bulletin, v. 109, p. 728–745.

Oskin, M., Stock, J., and Martín-Barajas, A., 2001, Rapid localization of Pacific-North American plate motion in the Gulf of California: Geology, v. 29, p. 459–462.

Roldan-Quintana, J., 1991, Geology and chemical composition of the Jaralito and Aconchi batholiths in east-central Sonora, *in* Perez-Segura, E., and Jacques-Ayala, C., eds., Studies of Sonoran geology: Boulder, Colorado, Geological Society of America Special Paper 254, p. 69–80.

Ruiz, J., Patchett, P.J., and Ortega-Gutiérrez, F., 1988, Proterozoic and Phanerozoic basement terranes of México from Nd isotopic studies: Geological Society of America Bulletin, v. 100, p. 274–281.

Sawlan, M.G., 1991, Magmatic evolution of the Gulf of California rift, *in* Dauphin, J.P., and Simoneit, B.A., eds., The Gulf and Peninsular Province of the Californias: American Association of Petroleum Geologists Memoir, v. 47, p. 301–369.

Schaaf, P., Moran-Zenteno, D., Hernandez-Bernal, M.d.S., Solis-Pichardo, G., Tolson, G., and Kohler, H., 1995, Paleogene continental margin truncation in southwestern México: Geochronological evidence: Tectonics, v. 14, p. 1339–1350.

Schaaf, P., Boehnel, H., and Perez-Venzor, J.A., 1997, Isotopic data on Los Cabos and Jalisco block granitoids: Paleogeographic implications [abs.]: Eos (Transactions, American Geophysical Union), v. 78, p. F844.

Schaaf, P., Boehnel, H., and Perez-Venzor, J.A., 2000, Pre-Miocene palaeogeography of the Los Cabos block, Baja California Sur: Geochronological and palaeomagnetic constraints: Tectonophysics, v. 318, p. 53–69.

Sedlock, R.L., Ortega-Gutiérrez, F., and Speed, R.C., 1993, Tectonostratigraphic terranes and tectonic evolution of México: Boulder, Colorado, Geological Society of America Special Paper 278, 153 p.

Sillitoe, R.H., 1976, A reconnaissance of the Mexican porphyry copper belt: Institute of Mining and Metallurgy Transactions, v. 85, p. B170-B189.

Silver, L.T., 1963, The relation between radioactivity and discordance in zircons: National Academy of Science, National Research Council, Nuclear Geophysics Publication 1075, p. 34–42.

Silver, L.T., and Chappell, B.W., 1988, The Peninsular Ranges batholith: An insight into the evolution of the Cordilleran batholiths of southwestern North America: Transactions of the Royal Society of Edinburgh: Earth Sciences, v. 79, p. 105–121.

Silver, L.T., Taylor, H.P., Jr., and Chappell, B., 1979, Some petrological, geochemical and geochronological observations of the Peninsular Ranges batholith near the International Border of the U.S.A., and México, *in* Abbott, P.L., and Todd, V.R., eds., Mesozoic crystalline rocks—Peninsular Ranges batholith and pegmatites, Point Sal ophiolite, *in* Geological Society of America Annual Meeting Guidebook: San Diego, San Diego State University, p. 83–110.

Smith, D.M., Albinson, T., and Sawkins, F.J., 1982, Geologic and fluid inclusion studies of the Tayoltita silver-gold vein deposit, Durango, México: Economic Geology, v. 77, p. 1120-1145.

Snee, L.W., Naeser, C.W., Naeser, N.D., Todd, V.R., and Morton, D.M., 1994, Preliminary $^{40}Ar/^{39}Ar$ and fission-track cooling ages of plutonic rocks across the Peninsular Ranges batholith, southern California: Geological Society of America Abstracts with Programs, v. 26, no. 2, p. A94.

Staude, J.-M.G., and Barton, M.D., 2001, Jurassic to Holocene tectonics, magmatism, and metallogeny of northwestern México: Geological Society of America Bulletin, v. 113, p. 1357–1374.

Steiger, R.H., and Jäger, E., 1977, Subcommission on geochronology: Convention on the use of decay constants in geo- and cosmochronology: Earth and Planetary Science Letters, v. 36, p. 359–362.

Stein, G., LaPierre, H., Monod, O., Zimmermann, J.L., and Vidal, R., 1994, Petrology of some Mexican Mesozoic-Cenozoic plutons: Sources and tectonic environments: Journal of South American Earth Sciences, v. 7, p. 1–7.

Stock, J.M., and Hodges, K.V., 1989, Pre-Pleistocene extension around the Gulf of California and the transfer of Baja California to the Pacific Plate: Tectonics, v. 8, p. 99–115.

Stock, J., and Molnar, P., 1988, Uncertainties and implications of the Late Cretaceous and Tertiary positions of North America relative to the Farallon, Kula, and Pacific plates: Tectonics, v. 7, p. 1339-1384.

Swanson, E.R., and McDowell, F.W., 1984, Calderas of the Sierra Madre Occidental volcanic field, western México: Journal of Geophysical Research, v. 89, p. 8787-8799.

Swanson, E.R., Keizer, R.P., Lyons, J.I., and Clabaugh, S.E., 1978, Tertiary volcanism and caldera development near Durango City, Sierra Madre Occidental, México: Geological Society of America Bulletin, v. 89, p. 1000–1012.

Tardy, M., Lapierre, H., Freydier, C., Coulon, C., Gill, J.B., Mercier de Lepinay, B., Beck, C., Martinez, R.J., Talavera, M.O., Ortiz, H.E., Stein, G., Bourdier, J.L., and Yta, M., 1994, The Guerrero suspect terrane (western México) and coeval arc terranes (the Greater Antilles and the western Cordillera of Colombia): A late Mesozoic intra-oceanic arc accreted to cratonal America during the Cretaceous: Tectonophysics, v. 230, p. 49–73.

Tate, M.C., Norman, M.D., Johnson, S.E., Fanning, C.M., and Anderson, J.L., 1999, Generation of tonalite and trondhjemite by subvolcanic fractionation and partial melting in the Zarza Intrusive Complex, western Peninsular Ranges batholith, northwestern México: Journal of Petrology, v. 40, p. 983–110.

Todd, V.R., and Shaw, S.E., 1979, Structural, metamorphic and intrusive framework of the Peninsular Ranges batholith in southern San Diego County, California, *in* Abbott, P.L., and Todd, V.R., eds., Mesozoic crystalline rocks—Peninsular Ranges batholith and pegmatites, Point Sal ophiolite: Geological Society of America Annual Meeting Guidebook: San Diego, San Diego State University, p. 177–232.

Todd, V.R., Erskine, B.G., and Morton, D.M., 1988, Metamorphic and tectonic evolution of the northern Peninsular Ranges batholith, southern California, *in* Ernst, W.G., ed., Metamorphism and crustal evolution of the western United States, Rubey Volume VII: Englewood Cliffs, New Jersey, Prentice-Hall, p. 894–937.

Tullis, J., 1983, Deformation of feldspars, *in* Ribbe, P.H., ed., Feldspar mineralogy: Mineralogical Society of America Reviews in Mineralogy, v. 2, p. 297–323.

Valencia-Moreno, M., Ruiz, J., Barton, M.D., Patchett, P.J., Zurcher, L., Hodkinson, D.G., and Roldan-Quintana, J., 2001, A chemical and isotopic study of the Laramide granitic belt of northwestern México: Identification of the southern edge of the North American Precambrian basement: Geological Society of America Bulletin, v. 113, p. 1409–1422.

Vernon, R.H., 1991, Questions about myrmekite in deformed rocks: Journal of Structural Geology, v. 13, p. 979–985.

Walawender, M.J., and Smith, T.E., 1980, Geochemical and petrologic evolution of the basic plutons of the Peninsular Ranges batholith, southern California: Journal of Geology, v. 88, p. 233–242.

Walawender, M.J., Gastil, R.G., Clinkenbeard, J.P., McCormick, W.V., Eastman, B.G., Wardlaw, R.S., Gunn, S.H., and Smith, B.M., 1990, Origin and evolution of the zoned La Posta-type plutons, eastern Peninsular Ranges batholith, southern and Baja California, *in* Anderson, J.L., ed., The nature and origin of Cordilleran magmatism: Boulder, Colorado, Geological Society of America Memoir 174, p. 1–18.

Walawender, M.J., Girty, G.H., Lombardi, M.R., Kimbrough, D., Girty, M.S., and Anderson, C., 1991, A synthesis of recent work in the Peninsular Ranges batholith, *in* Walawender, M.J., and Hanan, B.B., eds., Geological excursions in southern California and México: San Diego, San Diego State University, p. 297–317.

Wisser, E., 1965, The epithermal precious metal province of northwest México: Nevada Bureau of Mines Report 13, Part C, p. 63–92.

Zimmermann, J.L., Stussi, J.M., Gonzalez-Partida, E., and Arnold, M., 1988, K-Ar evidence for age and compositional zoning in the Puerto Vallarta–Rio Santiago batholith (Jalisco, México): Journal of South American Earth Sciences, v. 1, p. 267–274.

Manuscript Accepted by the Society June 2, 2003

Printed in the USA